Supporting Information

Graphite Conjugation Eliminates Redox Intermediates in Molecular Electrocatalysis

Megan N. Jackson, Corey J. Kaminsky, Seokjoon Oh, Jonathan F. Melville, Yogesh Surendranath*

Department of Chemistry, Massachusetts Institute of Technology, Cambridge, Massachusetts 02139, United States

*yogi@mit.edu

Table of contents

Materials and Methods

Chemicals and materials. Sodium hydroxide (99.99%, semiconductor grade), sodium formate (99.0%, BioUltra), sodium phosphate monobasic (TraceSELECT, anhydrous, 99.995% trace metals basis), sodium phosphate dibasic (TraceSELECT, anhydrous, 99.999% trace metals basis), and *o*-phenylenediamine (99.5%) were obtained from Sigma Aldrich and were used as received. Boric acid (Puratronic, 99.9995% trace metals basis) was purchased from Alfa Aesar, sulfuric acid (95.5-96.5%, OmniTrace) was obtained from EMD Millipore, and perchloric acid (Suprapur 70%, 99.999% trace metals basis) was obtained from Merck and used as received. All aqueous electrolyte solutions were prepared with reagent grade water (Millipore Type 1, 18.2 MΩ-cm resistivity). Dimethylformamide (EMD Chemicals) was purified and dried prior to use by passing through a Glass Contour Solvent Purification System (SG Water USA, LLC). Ethanol (absolute, dried, Seccosolv) was supplied by MilliPore Sigma and was stored and used in an N_2 glovebox. Glassy carbon disk electrodes were obtained from Pine Research Instrumentation, Inc. Vitreous carbon plates were obtained from Goodfellow (VC000400). Ag/AgCl reference electrodes were obtained from eDAQ. Platinum wire (99.9%) and Platinum mesh (99.9%) were obtained from Alfa Aesar. All syntheses were performed in solvent of ACS grade or better. The pH of aqueous electrolytes was adjusted with 1 M NaOH and 1 M $HClO_4$. Details of other chemical reagents used in syntheses are included in the synthetic protocols below.

General electrochemical methods. All electrochemical experiments were conducted at ambient temperature (21 ± 1 ˚C) using a Gamry REF 600 potentiostat or Biologic VSP potentiostat. All electrochemical experiments were conducted in a two-compartment electrochemical cell with a fine frit separating the working and auxiliary compartments. A platinum mesh was used as the counter electrode in the separated auxiliary compartment. Leakless aqueous Ag/AgCl (eDAQ) were used as the reference electrode. Ag/AgCl electrodes were stored in reagent-grade water and were periodically checked relative to pristine reference electrodes to ensure against potential drift. All electrode potentials are plotted vs the normal hydrogen electrode (NHE, $E_{NHE} = E_{Ag/AgCl} + 0.198$ V).

Preparation of GCCs.

Electrode cleaning and pre-treatment

Two types of graphitic carbon electrodes were used: 5 mm diameter glassy carbon disk electrodes and glassy carbon plates. Glassy carbon disk electrodes were polished using a Buehler MetaServ 250 Grinder/Polisher equipped with a Buehler Vector LC 250 rotating head. The electrodes were placed in custom fabricated PTFE holders and polished against a rotating ChemoMet (JH Technologies) surface with an alumina slurry for two minutes with 2 lbs of applied pressure, followed by rinsing with reagent-grade water. This process was repeated in sequence using 1.0 μm, 0.3 μm, and 0.05 μm alumina slurries, each on a different ChemoMet plate. Finally, the electrodes were sonicated in reagent-grade water. In order to increase the surface area and expose more quinone moieties, glassy carbon disk electrodes were anodized via potentiostatic electrolysis at 3.5 V vs RHE for 10 seconds in 0.1 M H_2SO_4. Electrodes were subsequently washed with copious amounts of reagent-grade water and ethanol and dried in vacuo prior to electrochemical evaluation or further functionalization.

Glassy carbon plates were only functionalized once and were used as received, without polishing. Where specified, to increase the population of quinone moieties on the surface, these electrodes were anodized via potentiostatic electrolysis at 3.5 V vs RHE for 10 seconds in 0.1 M H_2SO_4 and washed with copious amounts of reagent-grade water and ethanol prior to functionalization.

Preparation of GCC-Rh

Surface functionalization was carried out by immersing graphitic carbon electrodes (plates and disks) in ~10 mL of 1 mM [RhCp*(phenda)Cl]Cl (synthetic details below) in dry dimethylformamide in an N_2 glovebox. The reaction vessel was subsequently sealed under inert atmosphere, removed from the glovebox, and heated under N_2 for 10 hours at 110˚C. Upon cooling, the solution was decanted and the electrodes were washed with copious amounts of pure ethanol and subsequently treated with 0.1 M $HClO_4$ for 1 hour to hydrolyze adventitious imine linkages formed on the surface. Following acid treatment, electrodes were rinsed with water and dried in a 60˚C oven. This preparation was used to collect all characterization, cyclic voltammetry, and X-ray absorption data in this study.

Preparation of GCC-phenazine

GCC-phenazine was prepared via two methods. Unless otherwise specified, to compare directly to the surface preparation used for GCC-Rh, GCC-phenazine surface functionalization was carried out by immersing glassy carbon plates in ~10 mL of 1 mM *o*-phenylenediamine in dry dimethylformamide in an N_2 glovebox. The reaction vessel was subsequently sealed under inert atmosphere, removed from the glovebox, and heated under N_2 for 10 hours at 110˚C. Upon cooling, the solution was decanted and the electrodes were treated as described above: they were washed with copious amounts of pure ethanol and subsequently treated with 0.1 M $HClO_4$ for 1 hour. Following acid treatment, electrodes were rinsed with water and dried in a 60˚C oven. These phenazine modified electrode were used to record the background CV traces in **Figures 2 d**, **e**, and **f**.

To obtain higher coverages of surface phenazine units, glassy carbon electrodes were immersed in ~10 mL of 1 mM *o*-phenylenediamine in dry ethanol in an N_2 glovebox. The reaction vessel was subsequently sealed under inert atmosphere, removed from the glovebox, and heated

under N_2 for 10 hours at 60˚C. Upon cooling, the solution was decanted and the electrodes were washed with copious amounts of pure ethanol and subsequently treated with 0.1 M $HClO_4$ for 1 hour to hydrolyze adventitious imine linkages formed on the surface. Following acid treatment, electrodes were rinsed with water and dried in a 60˚C oven. This procedure was used to create the comparison electrode in **Figure S6**, which shows that the phenazine units do not promote hydrogen evolution.

Steady-state HER (Tafel) data collection on GCC-Rh.

Steady-state data were collected on GCC-Rh plates that were not anodized prior to functionalization. Data were collected in 20 mV increments between −0.4 V and −0.2 V vs NHE in 0.1 M $HClO_4$ (**Figure 3a**) and between −1.2 V and −1.0 V vs NHE in 0.1 M NaOH (**Figure S21**). Steady-state data were also collected on plates that were not anodized spanning ~2 V in 20 mV increments in electrolytes of varying pH to extract turnover frequency values for GCC-Rh (**Figures S7-S11**). Each potential was held for 10 s, although steady-state current was typically reached in < 1 s. Returning to the initial potential of polarization led to only a slight change in current density (0.2 decade change in 0.1 M $HClO_4$ and 0.1 decade change in 0.1 M NaOH), suggesting that the electrochemical activity did not change dramatically during the course of steady-state data collection (**Figures S22** and **S23**). Data collected on functionalized rotating disk electrodes at 0 rotations per minute (rpm) and 2000 rpm overlay, indicating that that the rate of HER was not gated by diffusion (**Figures S24** and **S25**).[1]

Turnover frequency calculations for GCC-Rh.

We calculated the turnover frequencies (TOFs) for GCC-Rh plotted in the potential-pH plot (**Figure 3**, blue dots) by using the steady-state Tafel data shown in **Figures S7-S11**. For each steady-state Tafel data point, the measured current density was normalized to the surface concentration of Rh by (1) integrating the charge in the phenazine wave for that electrode and (2) dividing by two, since the electrochemical reaction that occurs at the phenazine linkage in H_2O is a 2 H^+, 2 e^- process. The resulting frequency was then divided by two again to calculate the TOF per molecule of H_2 (since HER is a two-electron process) in s^{-1}. For each buffer, these values were plotted vs potential, giving rise to Tafel plots with TOF values. These plots were interpolated to find the potentials corresponding to TOF values of 1 s^{-1} for each electrolyte. The potential values are shown in the Pourbaix diagram (**Figure 3**, blue dots) and are the averages of two independently prepared electrodes.

XPS measurements and curve fitting.

X-ray photoelectron spectroscopy was conducted on anodized GCC-Rh electrodes after polarization at ~0.45 V overpotential for 10 minutes in the specified electrolyte. Electrodes were mounted to the platen with conductive carbon tape.

X-ray photoelectron spectra of GCC-Rh were recorded using a Physical Electronics PHI Versaprobe II with a monochromatic aluminum Kα X-ray source (1486.6 eV) and a hemispherical energy analyzer. Data were collected at a base pressure of 5×10^{-9} torr using a 200 μm, 50 W focused beam at a take-off angle of 45°. Survey spectra were collected using a pass energy of 187.85 eV and a step size of 0.8 eV. High-resolution scans were collected with a pass energy of 23.50 eV and a step size of 0.10 eV. Quantification was performed on the high-resolution scans using MultiPak software. Prior to quantification, the scans were smoothed with a 7-point Savitzky-Golay method. All other processing of the spectra was performed using CasaXPS. Both survey and high-resolution scans were smoothed with a 5-point Savitzky-Golay method and referenced to the graphitic C 1s peak (284.3 eV) of glassy carbon. High-resolution Rh 3d spectra were fit with linear backgrounds and two peaks of Gaussian/Lorentzian line-shapes of 30% Gaussian shape. N 1s spectra were fit with a Shirley type background and fit with two peaks of Gaussian/Lorentzian line-shapes of 30% Gaussian shape. The two peaks fit to the N1s manifolds were constrained to have equal areas (**Figure S17**).

The XPS data together indicate that GCC-Rh maintains its molecular fidelity after 10 minutes of hydrogen evolution catalysis in 0.1 M perchloric acid, 0.1 M sodium formate, 0.1 M sodium phosphate, 0.1 M sodium borate, and 0.1 M sodium hydroxide. Survey spectra indicate incorporation of Rh and N and show that there was no significant incorporation of metal impurities in the electrolyte during catalysis (**Figures S12-16**). Quantification from high-resolution XPS data for Rh $3p_{3/2}$ and N 1s gave rise to N:Rh ratios of ~4:1, in line with expected values (**Table S1**). High-resolution N 1s XPS on GCC-Rh were fit to two peaks in a 1:1 ratio at 399.9 and 399.0 eV (**Figure S17**), consistent with the expected binding energies for metal-bound pyridinic N and pyrazinic N. The Rh $3d_{5/2}$ peaks were centered around 309.3 eV, consistent with Rh^{III} (**Figure S18** and **Table S2**). This Rh binding energy is 2.3 eV positive of the expected XPS $3d_{5/2}$ peak for Rh^0,[2] suggesting that there is no formation of Rh nanoparticles during electrolysis.

Discussion of possible mechanisms of HER and corresponding transfer coefficients.

The derivations shown here have been previously discussed in the literature.[3–6]

Here, we discuss the potential-dependence for each of three possible mechanistic pathways for HER at GCC-Rh: two-electron transfer followed by rate-limiting proton transfer (EEC), one-electron transfer followed by rate-limiting proton-transfer (EC), and rate-limiting proton-coupled electron transfer (CPET).

Pathway	Possible α values	Possible Tafel slopes (mV dec^{-1})
EEC	2	30
EC	1	60
CPET	0-1	> 60

Two-electron transfer followed by rate-limiting proton transfer (EEC mechanism):

In this case, we consider a pathway in which the Rh site is first reduced by two electrons, followed by a proton transfer step:

Step 1: $Rh^{III} + 2e^- \underset{k_{-1}}{\overset{k_1}{\rightleftharpoons}} Rh^I$

Step 2: $Rh^I + H^+ \overset{k_2}{\rightarrow} Rh - H$ (**rate-determining step**)

in which k_1, k_{-1}, and k_2 are rate constants for the elementary steps.

In this case, the rate law is the following:

$$rate = k_2[Rh^I][H^+]$$

To write this rate expression as a function of starting material, we assume that Step 1 is in rapid pre-equilibrium. The concentration of $[Rh^I]$ is thus governed by the Nernst equation:

$$\eta = \left| -\frac{RT}{nF} \ln\left(\frac{[Rh^I]}{[Rh^{III}]}\right) \right|$$

$$\Rightarrow [Rh^I] = [Rh^{III}] \exp\left(\frac{n\eta F}{RT}\right)$$

where n is the number of electrons in the redox process, η is the overpotential for the electron transfer step, F is Faraday's constant, R is the gas constant, and T is the temperature. Subbing in for the original rate expression, we get:

$$rate = k_2[Rh^{III}][H^+] \exp\left(\frac{n\eta F}{RT}\right)$$

To obtain the expected Tafel slope for this mechanism, we take the derivative of the overpotential with respect to the rate. Since rate is proportional to current density in mA, j, we can write this relationship as the derivative of the overpotential with respect to current density and solve for a two-electron redox process at room temperature:

$$\frac{\delta\eta}{\delta \log(j)} = 2.3\frac{RT}{nF} = 30\ mV\ dec^{-1}$$

We note that this potential dependence would be observed for *any* mechanistic sequence in which two-electron reduction of the catalyst resting state is followed by a rate-limiting chemical step.

One-electron transfer followed by rate-limiting proton transfer (EC mechanism):

In this pathway, we assume one-electron reduction of the Rh site, followed by rate-limiting proton transfer:

$$\textbf{Step 1: } Rh^{III} + e^- \underset{k_{-1}}{\overset{k_1}{\rightleftharpoons}} Rh^{II}$$

$$\textbf{Step 2: } Rh^{II} + H^+ \overset{k_2}{\rightarrow} Rh - H \textbf{ (rate-determining step)}$$

This derivation follows the same analysis described above for the EEC mechanism, except n = 1. The potential dependence for n=1 at room temperature is the following:

$$\frac{\delta\eta}{\delta\log(j)} = 2.3\frac{RT}{F} = 60\ mV\ dec^{-1}$$

Again, this potential dependence would be observed for any mechanistic sequence in which one-electron reduction of the catalyst resting state is followed by a rate-limiting chemical step.

Rate-limiting concerted proton-coupled electron transfer (CPET mechanism):

We now consider a pathway in which the first step after the catalyst resting state is a concerted proton-coupled electron transfer step:

Step 1: $Rh^{III} + e^- + H^+ \rightleftharpoons Rh - H$ **(rate-determining step)**

In this case, the rate law is the following:

$$rate = k[Rh^{III}][H^+]\exp\left(\frac{\eta\beta F}{RT}\right)$$

Where β is the symmetry factor, and all other symbols take on their previously stated meanings. To determine the potential dependence, we write:

$$\frac{\delta\eta}{\delta\log(j)} = 2.3\frac{RT}{\beta F}$$

Typically, β = 0.5, and we expect a Tafel slope of 120 mV dec^{-1}, but β can range from 0 to 1, and any value greater than 60 mV dec^{-1} is consistent with this pathway. [1,7]

GCC-Rh displays a Tafel slope of 110 mV dec^{-1} in 0.1 M $HClO_4$ (**Figure 3a**) and 200 mV dec^{-1} in 0.1 M NaOH (**Figure S21**), which are both consistent with rate-limiting electron transfer. We note that Tafel slopes greater than 60 dec^{-1} are consistent with any pathway in which the first electron transfer step from the catalyst resting state is rate-limiting, even if it is not proton-coupled. However, the observation of an H/D kinetic isotope effect of 2.0 for HER at GCC-Rh suggests that GCC-Rh proceeds through a pathway in which the first *concerted* proton-electron transfer step is rate-determining.

H/D kinetic isotope effect.

$HClO_4$ electrolytes (1 M) were prepared by adding 1.73 mL concentrated $HClO_4$ (EMD Millipore, Suprapur) to 18.27 mL H_2O or D_2O (Cambridge Isotope Laboratories, Inc, 99.9%) to make 20 mL electrolyte total. To measure the H/D kinetic isotope effect (KIE) for H_2 evolution at GCC-Rh, we took slow-scan cyclic voltammograms (CVs, 5 mV s^{-1}) in each electrolyte with 3 independently prepared GCC-Rh disk electrodes. Representative CVs in H_2O and D_2O electrolyte are shown in **Figure 3b**. Since CVs recorded at 5 mV s^{-1} and 1 mV s^{-1} give rise to the same slope on a log plot (**Figures S26** and **S27**), we conclude that 5 mV s^{-1} is a slow enough scan rate for the system to reach steady-state in pH 0 electrolyte. We note that plots of the applied potential vs the log of the current density (Tafel plots) of the slow scan CVs in H_2O and D_2O had the same slope (80 mV dec^{-1}, **Figure S27**), suggesting that there is no potential dependence to the H/D KIE under these conditions.

Since the D_2O electrolyte was prepared with concentrated $HClO_4$, it was only 91% D, so taking the ratio of the rate of HER in the H_2O and D_2O electrolytes does not fully measure the H/D KIE. We can solve for the KIE with 100% D_2O as follows. Assuming independent H and D rate expressions, for any mixed H_2O/D_2O electrolyte, the rate expression is:

$$j_{tot} = j_H(x) + j_D(1 - x)$$

in which j_H represents the rate of the reaction from H_3O^+, j_D represents the rate of the reaction from D_3O^+, x is the mole fraction of H^+ in the electrolyte, and j_{tot} represents the overall rate of the reaction.

In H_2O electrolyte, $x = 1$, so $j_{tot} = j_H$ and we measure j_H directly. We can then use this value to solve for j_D in our experiments in which $x = 0.09$:

$$j_{tot} = j_H(x) + j_D(1 - x)$$

$$\Rightarrow j_D = \frac{j_{tot} - j_H(x)}{(1 - x)}$$

When x = 0.09:

$$j_D = \frac{j_{tot} - j_H(0.09)}{(0.91)}$$

The following results were obtained by averaging the H/D KIE (j_H/j_D from CVs) between −0.25 and −0.3 V vs NHE:

	GCC-Rh electrode 1	GCC-Rh electrode 2	GCC-Rh electrode 3	Average
j_H/j_D	2.17 ± 0.02	2.05 ± 0.02	1.92 ± 0.02	2.0 ± 0.1

X-ray absorption spectroscopy.

X-ray absorption spectroscopy (XAS) setup:

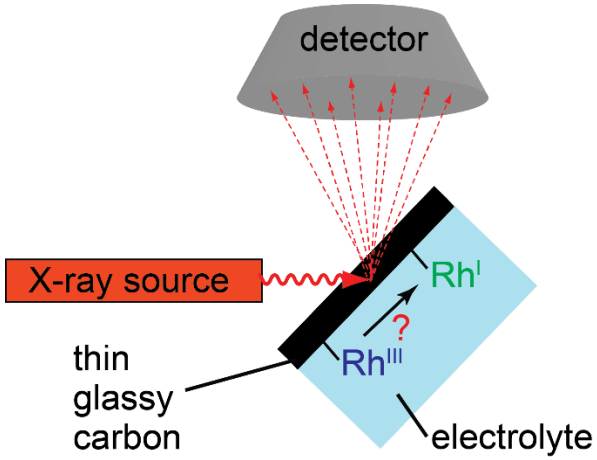

Scheme S1. Depiction of in situ X-ray absorption spectroscopy setup. Experimental details are below.

X-ray absorption spectroscopy.

X-ray absorption measurements were conducted on the insertion device beam line of the Materials Research Collaborative Access Team (MRCAT) at the Advanced Photon Source, Argonne National Laboratory. Spectra of Rh samples were collected at the Rh K-edge. Data for Rh standards were collected in transmission step scan mode. The ionization chambers were optimized for the maximum current with linear response (~3 x 10^{13} photons detected/sec) with 2.14% absorption (95% N_2-5% Ar) in the incident ion chamber and 2.14% absorption (N_2) in the transmission and reference X-ray detectors. The monochromator was aligned to Rh foil (23,220.0 keV). Sample preparation and collection parameters for specific samples are as follows.

GCC-Rh. GCC-Rh electrodes were prepared according the methods described above. After functionalization of the electrode, one side of each plate was exposed to concentrated nitric acid for 10 minutes so that only the side that would be exposed to electrolyte in the in situ cell remained functionalized. CVs in 0.1 M $HClO_4$ indicated that this exposure to nitric acid removed the phenazine units from the surface, and inductively coupled plasma mass spectrometry of nitric acid solution following dissolution of the metal on the electrode surface indicated that the metal had been removed. Using silicone adhesive, the electrode was then glued onto the window (10 mm diameter) on the working compartment of an H-cell with the functionalized side facing into the cell. The silicone was allowed to dry in air for at least 30 minutes before subsequent manipulation of the cell. The working and counter electrode chambers of the H-cell were separated by a porous glass frit. Each compartment was filled with aqueous electrolyte (0.1 M $HClO_4$ or 0.1 M NaOH). A high-surface area Pt mesh was used as the counter electrode, and Ag/AgCl was used as the reference electrode. The cell was sealed with rubber septa. Once aligned with the beam and the detector, both the working and auxiliary compartments were sparged with N_2 for at least 30 minutes prior to data collection and also during data collection. The sparge tubes were positioned such that bubbles would not interfere with the beam path.

XAS spectra were collected in fluorescence mode at a 10° glancing angle. A simplified rendering of the setup is shown in **Scheme S1**. The fluorescence was collected using a Lytle detector filled with Ar gas. Soller slits were used to minimize background.

The first derivative plots of the X-ray absorption near edge structure (XANES) spectra are in **Figures 3c** and **S29**.

[RhCp(phen)Cl]Cl*. Powder samples were diluted with BN and pressed into a cylindrical sample holder consisting of six wells, forming a self-supporting wafer which was then placed in a quartz tube (1 in. OD, 10 in. length) and sealed with Kapton windows using two Ultra-Torr fittings. Rh K-edge spectra were obtained in transmission mode at room temperature in air. The first derivative plot of the XANES spectrum is shown in **Figure S28**.

[RhCp(phen)]*. A benzene solution of RhCp*phen in benzene (90 mM) was prepared and sealed in an NMR tube under N_2. Rh K-edge spectra were obtained in transmission mode at room temperature. The first derivative plot of the XANES spectrum is shown in **Figure S28**.

All XANES data were processed using Athena software (Demeter 0.9.24).

Synthesis and characterization of molecular precursors and model compounds.

General characterization methods:
^{1}H and ^{13}C NMR spectra were recorded on a Bruker 400 MHz spectrometer or a JEOL 500 MHz spectrometer. All chemical shifts are reported in ppm and are referenced to tetramethylsilane (TMS) utilizing residual ^{1}H or ^{13}C signals of deuterated solvents as internal standards. Elemental analyses were carried out by Robertson Microlit Laboratories, Inc., Ledgewood, NJ. Mass spectra were recorded on a Bruker Autoflex Speed equipped with a reflectron accessory. Samples were prepared using 1,4-bis(5-phenyl-2-oxazolyl)benzene (POPOP, Alfa Aesar, 98+%) as the matrix, however; concurrent appearance of impurities in the spectrum resulted. These impurities were also present when POPOP was loaded on the target alone. A trace amount of *meso*-tetraphenylporphine was included as an internal standard.

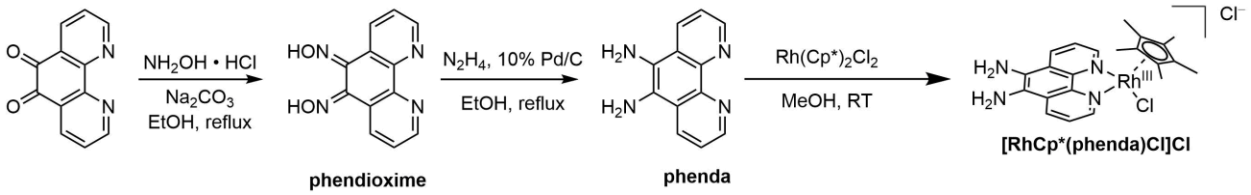

Scheme S2. Synthetic scheme for [RhCp*(phenda)Cl]Cl.

Synthesis of 1,10-phenanthroline-5,6-dioxime (phendioxime)
1,10-Phenanthroline-5,6-dioxime was synthesized following a literature procedure.[8] The reaction was performed under inert atmosphere. 1,10-phenanthroline-5,6-dione (770 mg, 3.66 mmol, 1 eq, Ark Pharm) and sodium carbonate (582 mg, 5.49 mmol, 1.5 eq, Macron Fine Chemicals) were added to ethanol (25 mL) and heated to reflux. Hydroxylamine hydrochloride (890 mg, 12.81 mmol, 3.5 eq, Sigma-Aldrich, 99%) dissolved in ethanol (45 mL) was added dropwise to the hot solution, and the reaction mixture was refluxed for 5 h. The mixture was then cooled and decanted into a new flask to minimize collection of the black solid that had formed at the bottom of the reaction flask. The solvent was removed *in vacuo* and the resulting solid was washed successively with 20 mL each of water and THF and dried *in vacuo* at 50 °C overnight. Yields ranged between 60-85%. The resulting product, a light-yellow solid, was used in subsequent synthetic steps without further purification.

Synthesis of 5,6-diamino-1,10-phenanthroline (phenda)
The following preparation was adapted from the method described by Bodige and MacDonnell.[9] The reaction and workup were performed under argon atmosphere. A slurry of 1,10-phenanthroline-5,6-dioxime (2530 mg, 10.5 mmol), Pd/C (1000 mg, 10% on activated carbon, Strem), and ethanol (300 mL) was purged with Ar, then heated to reflux. A mixture of 35 mL ethanol and 25 mL hydrazine monohydrate (Sigma-Aldrich) was added dropwise over 1 h and the reaction mixture was subsequently refluxed overnight. The hot mixture was then filtered through a bed of celite which was then washed 3 times with 15 mL each of hot ethanol. The solvent was removed from the filtrate *in vacuo*, and the resulting solid was triturated with water and left to sit overnight at 4 °C. The mixture was then filtered, washed with additional water, and dried *in vacuo* to produce 1.6 g (72%) of yellow powder. The product was stored under inert atmosphere. (Exposure to air led to slow decomposition over the course of several days, indicated by a color

change from yellow to brown.) ^{1}H-NMR(400 MHz, DMSO-d_6) δ (ppm): 8.78 (dd, 2H), 8.48 (dd, 2H), 7.62 (dd, 2H), 5.22 (s, 4H).

Synthesis of chlorocyclopentadienyl(5,6-diamino-1,10-phenanthroline)rhodium(III) chloride ([RhCp*(phenda)Cl]Cl)

Compound was prepared according a literature procedure[10] with slight modifications. Pentamethylcyclopentadienylrhodium(III) chloride dimer (50 mg, 80 μmol, Strem 99%) and 5,6-diamino-1,10-phenanthroline (33.7 mg, 160 μmol) were combined in 15 mL of methanol and stirred for 2 hours under inert atmosphere. The solvent was removed under reduced pressure by rotary evaporation and the solid was redissolved in a minimum amount of methanol. Diethyl ether was added and the resulting orange solid was filtered and collected. The product was stored under inert atmosphere. Yield: 115 mg (69%). ^{1}H-NMR(400 MHz, DMSO-d6) δ (ppm): 9.03 (d, 2H), 8.89 (d, 2H), 8.01 (dd, 2H), 5.90 (s, 4H), 1.70 (s, 15H). ^{13}C-NMR(400 MHz, DMSO-d6) δ (ppm): 147.71, 139.40, 132.08, 127.47, 124.23, 123.51, 97.07-96.99 (d), 8.97. Anal. Calcd. for $C_{22}H_{25}Cl_2N_4Rh$: C, 50.89; H, 4.85; N, 10.79. Found: C, 51.11; H, 4.85; N, 10.39.

Synthesis of chlorocyclopentadienylbathophenanthrolinedisulfonic acid disodium rhodium(III) chloride Na_2([RhCp*(bpds)Cl]Cl)

The compound was prepared by modification of a literature procedure.[10] Pentamethylcyclopentadienylrhodium(III) chloride dimer (100 mg, 0.162 mmol, Strem 99%) and bathophenanthrolinedisulfonic acid disodium salt trihydrate (167 mg, 0.324 mmol, Sigma-Aldrich 98%) were combined in 20 mL of methanol and stirred for 6 hours. The solvent was removed under reduced pressure by rotary evaporation and the solid was redissolved in a minimum amount of methanol. Diethyl ether was added and the resulting yellow-orange solid was filtered and washed with diethyl ether (213 mg, 81% yield). ^{1}H-NMR(400 MHz, D_2O) δ (ppm): 9.37 (t, 2H), 8.16-7.87 (m, 8H), 7.82-7.50 (m, 6H), 1.79 (s, 15H). ^{13}C-NMR(400 MHz, D_2O with one drop of 4 M NaOH for solubility) δ (ppm): 151.10, 150.11, 146.10, 143.65, 143.44, 138.30, 136.06, 132.74, 130.42, 129.86, 128.25, 127.15, 126.72, 126.53, 126.12, 125.30, 95.40, 7.38. Anal. Calcd. for $C_{34}H_{29}Cl_2N_2Na_2O_6RhS_2$: C, 48.30; H, 3.46; N, 3.31. Found: C, 47.79; H, 3.44; N, 3.20. We attribute the discrepancy between the C values to partial hydration of the complex. (Anal. Calcd. with additional H_2O equivalent: C, 47.29; H, 3.62; N, 3.24.)

Synthesis of chlorocyclopentadienylphenanthrolinerhodium(III) chloride ([RhCp*(phen)Cl]Cl)

The compound was prepared according to a literature procedure.[10] Pentamethylcyclopentadienylrhodium(III) chloride dimer (150 mg, 0.243 mmol, Strem 99%) and 1,10-phenanthroline (87.5 mg, 0.485 mmol, Alfa Aesar 99%, anhydrous) were combined in 15 mL of methanol and stirred for 1 hour. The solvent was removed under reduced pressure by rotary evaporation and the solid was redissolved in a minimum amount of methanol. Diethyl ether was added and the resulting orange solid was filtered and collected (287.8 mg, 47% yield). ^{1}H-NMR(400 MHz, $CDCl_3$) δ (ppm): 9.41 (d, 2H), 8.68 (d, 2H), 8.28 (t, 2H), 8.09 (s, 2H), 1.87 (s, 15H).

Synthesis of cyclopentadienyl(1,10-phenanthroline)rhodium(I) ([RhCp*(phen)]):

Though the 1,10-phenanthroline, [RhCp*(phen)], complex has been reported previously,[11,12] the procedure reported here is a modification of the literature procedure for the analogous bipyridine

complex.[13] Under an atmosphere of nitrogen, [RhCp*phenCl]Cl (28 mg, 0.057 mmol) was added to a vial charged with a stir bar and containing 4 ml of 1 M NaOH. While stirring, sodium borohydride (24 mg, 0.63 mmol, Fluka analytical, >99%) dissolved in 2 ml of 1 M sodium hydroxide (Fisher Chemical) was added resulting in a color change from yellow to green, followed by the immediate precipitation of a dark green solid. The reaction was allowed to stir for 2 hours at room temperature and the precipitate was collected on a sintered glass funnel. The solid was washed with 3 by 10 ml MilliQ water and then eluted with benzene (10 ml, deaerated with argon for 30 minutes prior to use). The solvent was removed *in vacuo* to yield [RhCp*(phen)] as a dark green solid (25 mg, 106% yield, attributed to residual benzene). ^{1}H-NMR (500 MHz, C_6D_6) δ (ppm): 9.33 (d, J=6.0 Hz, 2H), 7.35 (d, J=7.2 Hz, 2H), 7.19 (s, 2H), 6.83 (t, J=6.6 Hz, 2H), 1.93 (s, 15H).

Synthesis of dipyrido[3,2-a:2',3'-c]phenazine-11-sulfonic acid (dppz-SO_3):
A different synthesis of this molecule has been previously reported.[14] 1,10-Phenanthroline-5,6-dione (100 mg, 0.48 mmol, Ark Pharm, 98%) and 3,4-diaminobenzenesulfonic acid (90 mg, 0.48 mmol, Sigma Aldrich, ARK409819060) were combined in 10 mL ethanol and stirred at 60 ºC for 12 hours. The resulting tan precipitate was collected on a sintered glass funnel and washed with excess cold water, methanol and acetone. 126 mg of product (73% yield) were collected. ^{1}H-NMR (400 MHz, DMSO-d6) δ (ppm): 9.79 (d, 1H), 9.75 (d, 1H), 9.30 (d, 2H), 8.57 (s, 1H), 8.42 (d, 1H), 8.28 (d, 1H), 8.17 (dd, 2H).

Synthesis of cyclopentadienyl(dipyrido[3,2-a:2',3'-c]phenazine-11-sulfonic acid)rhodium(I) ([RhCp*(dppzSO_3)]):
The procedure reported here is a modification of the literature procedure for the analogous bipyridine complex.[13] Pentamethylcyclopentadienylrhodium(III) chloride dimer (100 mg, 0.16 mmol, Strem 99%) and dppzSO_3 (58 mg, 0.16 mmol) were combined in 10 mL of ethanol and stirred for 1 hour under inert atmosphere. Tan solid was filtered in a fume hood and collected (84 mg, 78% yield). Trace water in DMSO-d6 hydrolyzes the RhCl bond to form a mixture of the chloro and aquo species. Elemental Analysis: Anal. Calcd. for $C_{28}H_{25}N_4O_3Cl_2SRh$: C, 50.09; H, 3.75; N, 8.34. Anal. Calcd. for $C_{28}H_{24}N_4O_3ClSRh$ (loss of HCl to form zwitterionic complex): C, 52.97; H, 3.81; N, 8.82. Anal Calcd. for $C_{28}H_{26}N_4O_4ClSRh$ (monohydrated zwitterionic complex): C, 51.51; H, 4.01; N, 8.58. Found: C, 51.28; H, 3.62; N, 9.02. 1H-NMR, 13C-NMR, and MALDI data are on the following pages (S16-S18).

The equilibrium can be shifted by controlled addition of excess D_2O, as revealed by the change in ^{1}H-NMR spectra collected in the presence of 1 µL D_2O and 10 µL D_2O:

^{1}H-NMR (600 MHz, DMSO-d6 + 1 µL D_2O) δ (ppm): 9.85 & 9.81 & 9.77 (all d with *J*=8.1, 2H together), 9.48 (m, 1H), 9.31 (br. d, *J*=4.3, 1H), 8.59 & 8.57 (both d with *J*=1.7, 1H together), 8.46 & 8.42 (both d with *J*=8.7, 1H together), 8.38 (m, 1H), 8.31 & 8.27 (both dd with *J*=8.9 and *J*=1.6, 1H together), 8.18(br. m, 1H), 1.76 & 1.63 (both s, 15H together in ~1.2:1 ratio).

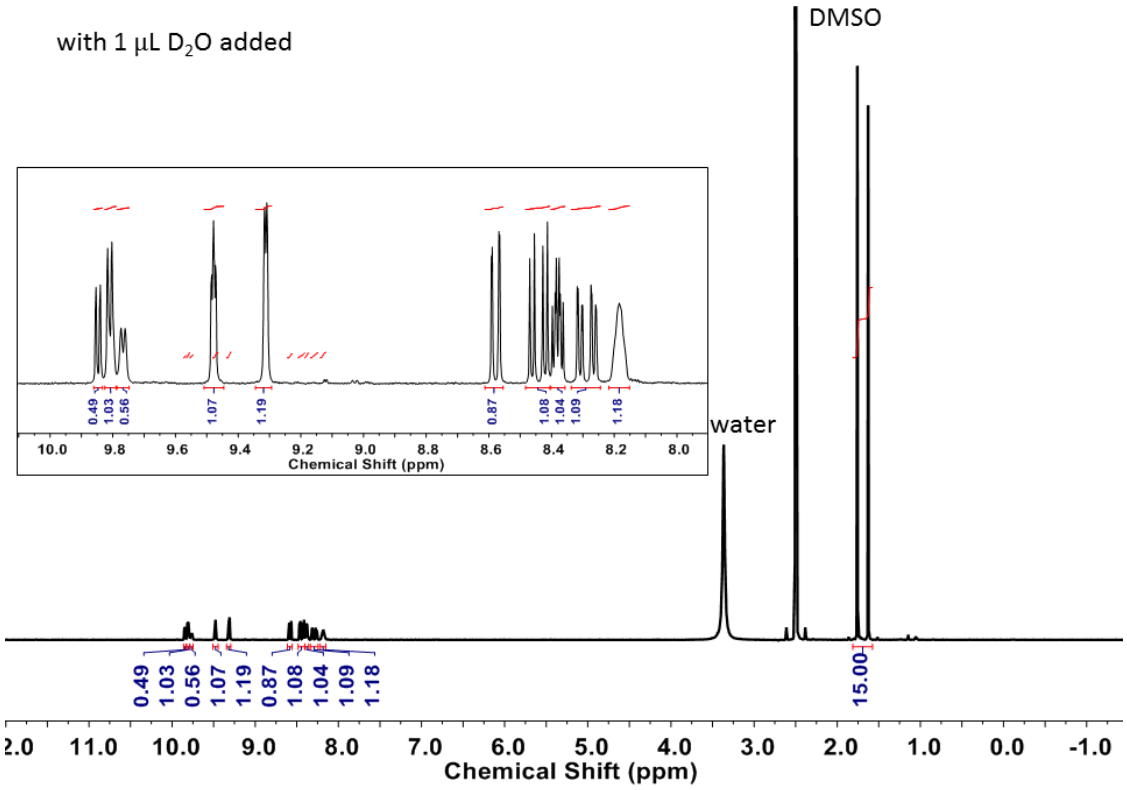

^{1}H-NMR (600 MHz, DMSO-d6 + 10 µL D_2O) δ (ppm): 9.84 (d, *J*=8.2, 1H), 9.80 (d, *J*=8.2, 1H), 9.47 (m, 2H), 9.32 (d, *J*=4.6, 1H), 8.59 & 8.58 (both d with *J*=1.6, 1H together), 8.46 & 8.43 (both d with *J*=8.8, 1H together), 8.38 (m, 1H), 8.31 & 8.29 (both dd, *J*=8.8, and *J*=1.7, 1H together), 8.23 (m, 1H), 1.75 & 1.62 (both s, 15H together in ~2.5:1 ratio).

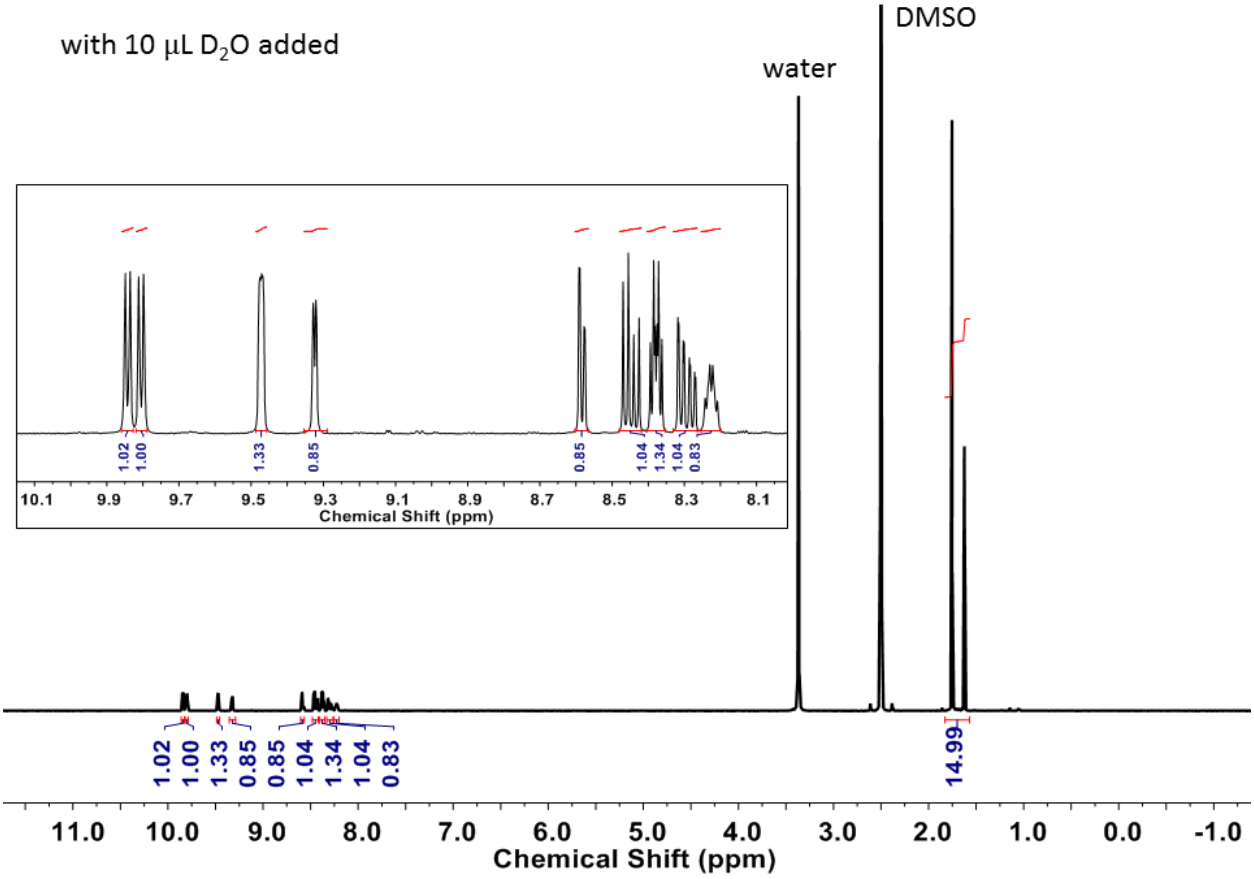

^{13}C-NMR (600 MHz, DMSO-d6) δ (ppm): 153.90, 153.88, 151.33, 147.68, 147.64, 141.87, 141.62, 139.92, 139.66, 135.86, 135.78, 130.64, 129.37, 129.33, 129.28, 128.42, 128.37, 124.86, 97.16 (d, $J_{C\text{-}Rh}$ = 6.33 Hz), 8.56.

MALDI: Two overlapping peak manifolds with 599.067 *m/z* and 699.077 *m/z* found, corresponding to $(M - 2Cl)^+$ with 599.062 *m/z* and $(M + H - 2Cl)^+$ with 600.070 *m/z* expected, respectively.

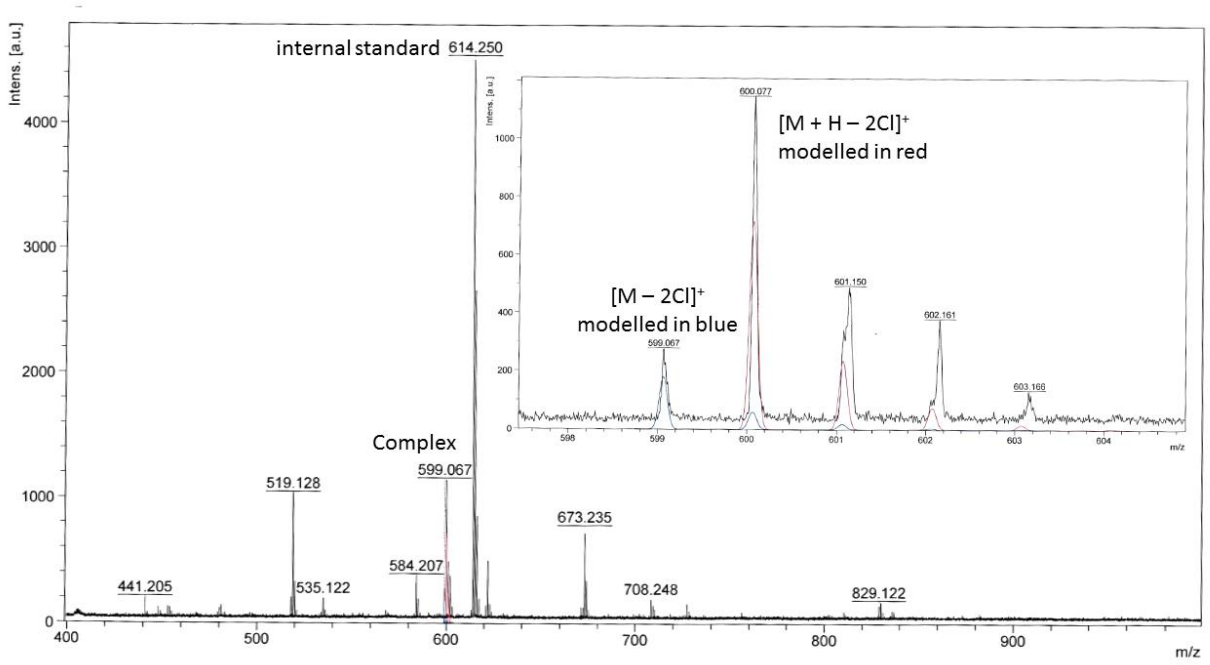

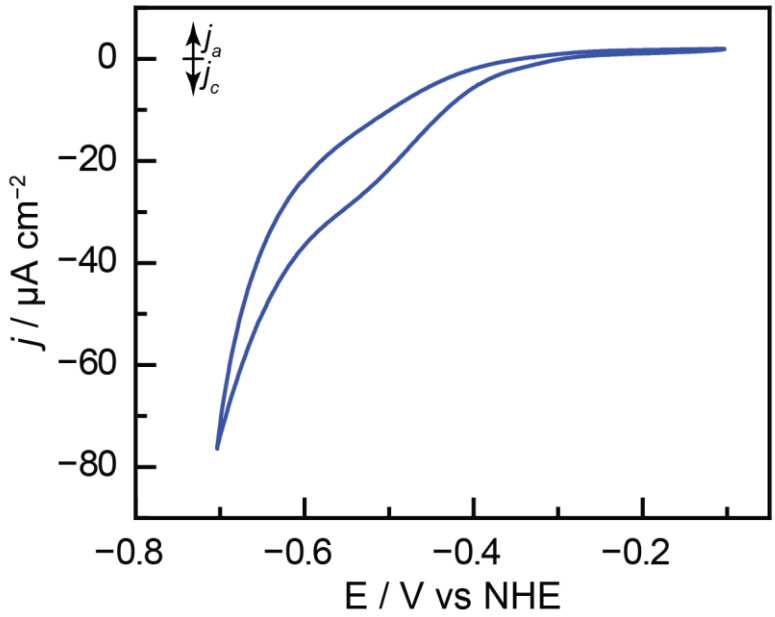

Figure S1. Cyclic voltammogram (10 mV s^{-1}) of 0.3 mM RhCp*(bpds)OH_2 recorded in 0.1 M sodium formate (pH 4.0).

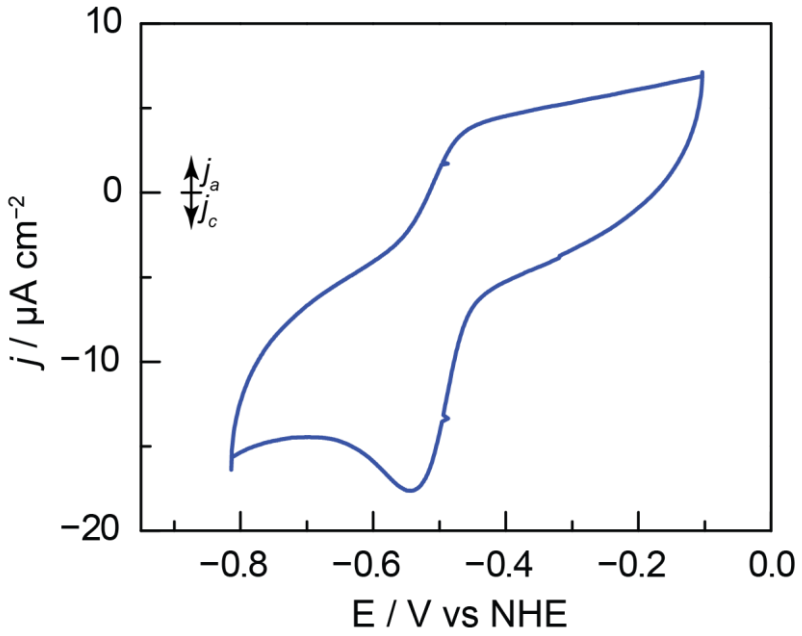

Figure S2. Cyclic voltammogram (10 mV s^{-1}) of 0.3 mM RhCp*(bpds)OH_2 recorded in 0.1 M sodium borate (pH 9.2).

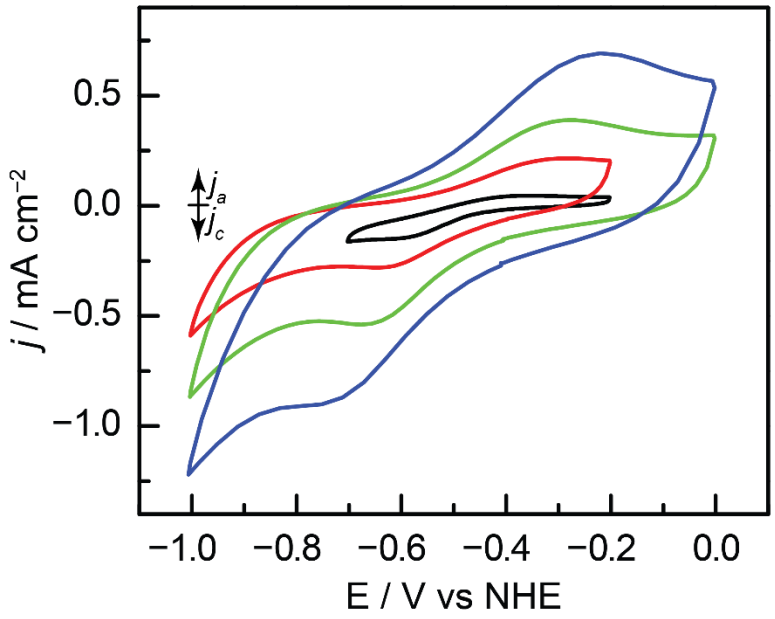

Figure S3. Cyclic voltammograms of 0.3 mM RhCp*(bpds)OH_2 recorded in 0.1 M sodium phosphate (pH 7.2) at 1 V s^{-1} (black), 5 V s^{-1} (red), 10 V s^{-1} (green), and 20 V s^{-1} (blue). $E_{1/2}(Rh^{III/I})$ in **Figure 2g** was obtained by averaging the minimum and maximum peak positions at 20 V s^{-1}.

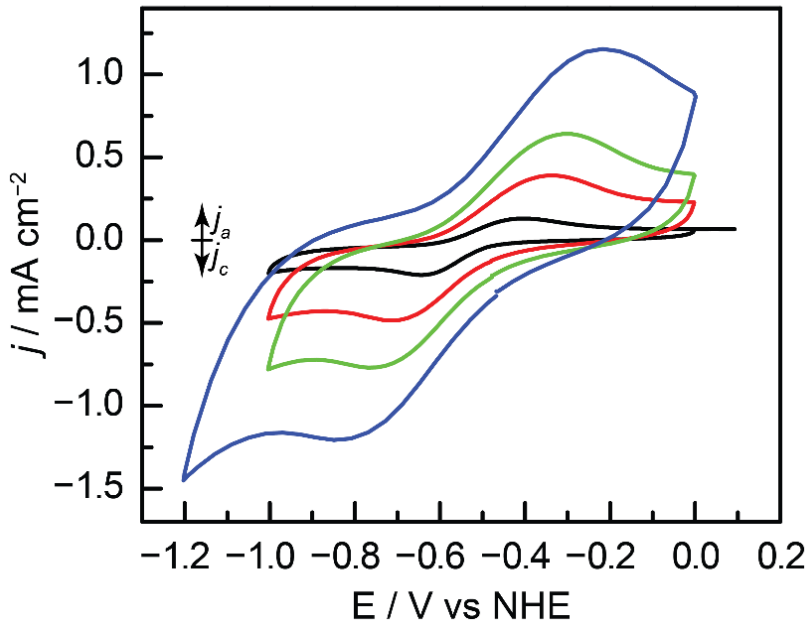

Figure S4. Cyclic voltammograms of 0.3 mM RhCp*(bpds)OH_2 recorded in 0.1 M sodium borate (pH 9.2) at 1 V s^{-1} (black), 5 V s^{-1} (red), 10 V s^{-1} (green), and 20 V s^{-1} (blue). $E_{1/2}(Rh^{III/I})$ in **Figure 2g** was obtained by averaging the minimum and maximum peak positions at 20 V s^{-1}.

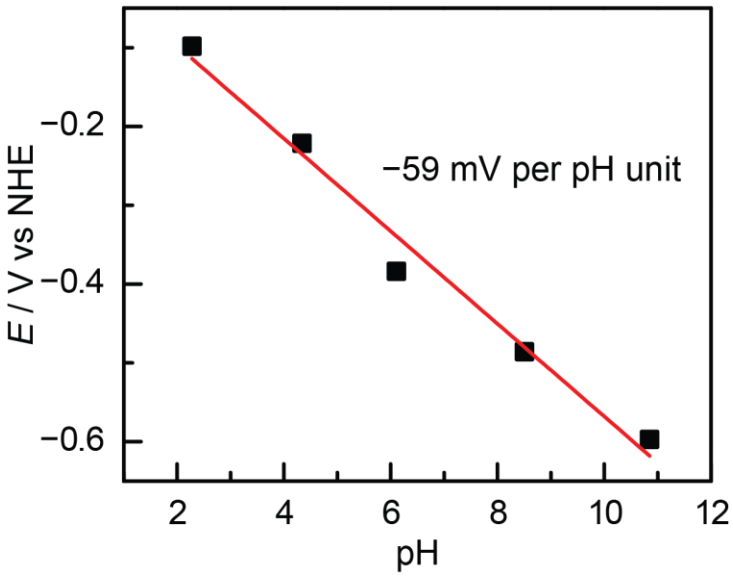

Figure S5. $E_{1/2}$ vs pH for GCC-Rh phenazine wave. CVs of GCC phenazine were recorded at 10 mV s^{-1} in 0.1 M sodium borate/0.1 M sodium phosphate/0.1 M sodium acetate aqueous electrolyte that was pH-adjusted with 1 M $HClO_4$ and 1 M NaOH. The slope of the best fit line is −59 mV per pH unit.

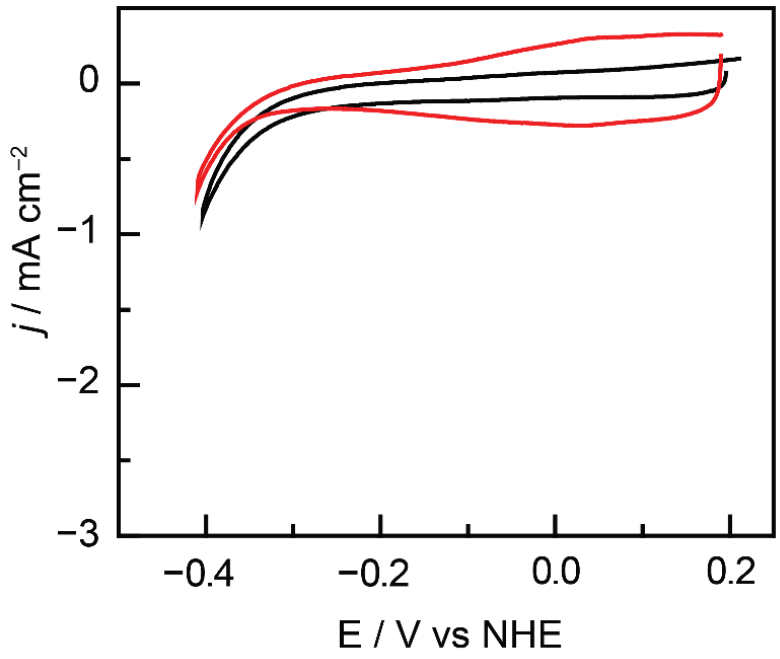

Figure S6. Cyclic voltammograms (10 mV s^{-1}) recorded in 0.1 M $HClO_4$ on an oxidized glassy carbon disk electrode pre-functionalization (black) and post-functionalization with *o*-phenylenediamine in ethanol to form GCC-phenazine.

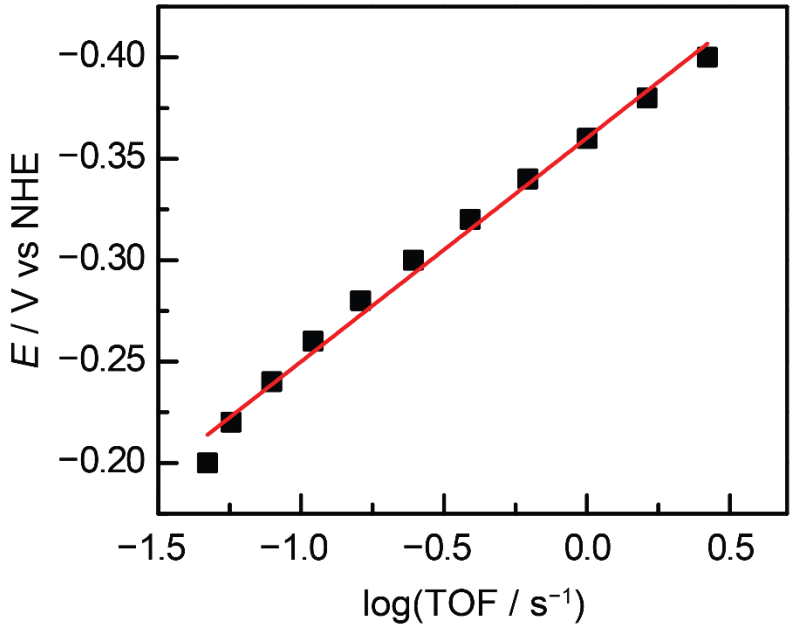

Figure S7. Average of two potentiostatic Tafel data runs for HER collected with GCC-Rh in 0.1 M $HClO_4$ electrolyte. The slope of the best fit line is 110 mV dec^{-1}.

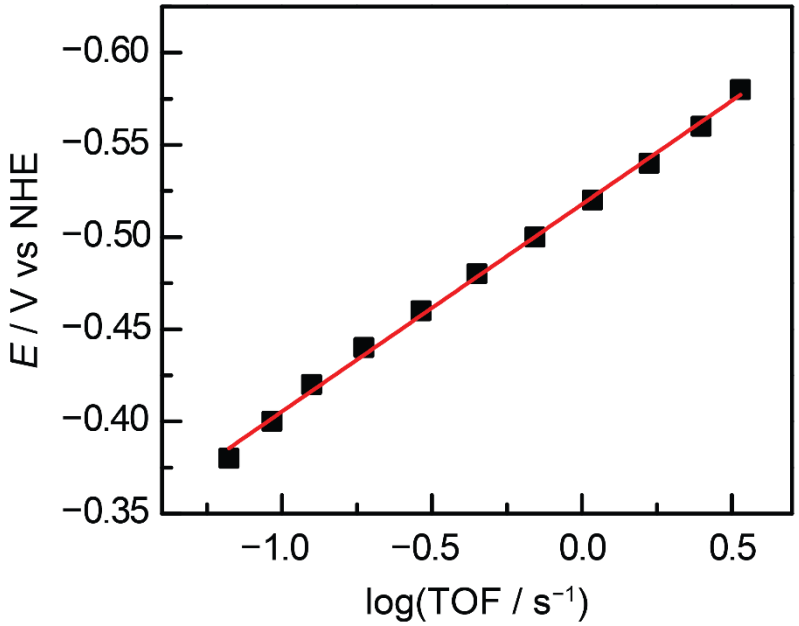

Figure S8. Average of two potentiostatic Tafel data runs for HER collected with GCC-Rh in 0.1 M sodium formate electrolyte. The slope of the best fit line is 112 mV dec^{-1}.

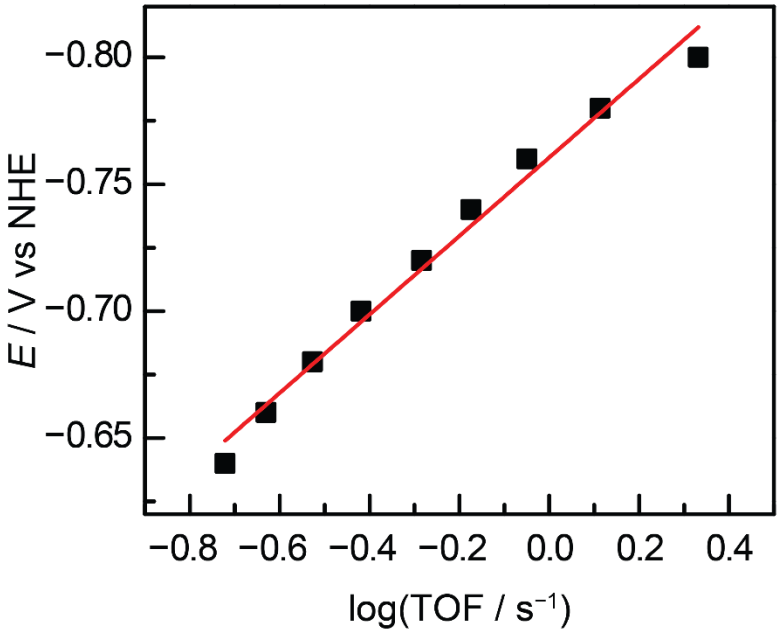

Figure S9. Average of two potentiostatic Tafel data runs for HER collected with GCC-Rh in 0.1 M sodium phosphate electrolyte. The slope of the best fit line is 154 mV dec^{-1}.

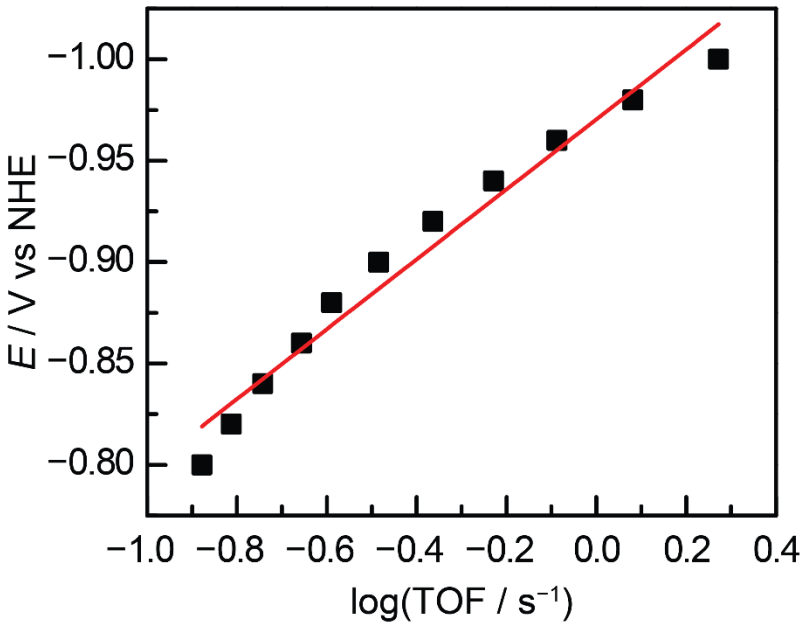

Figure S10. Average of two potentiostatic Tafel data runs for HER collected with GCC-Rh in 0.1 M sodium borate electrolyte. The slope of the best fit line is 172 mV dec^{-1}.

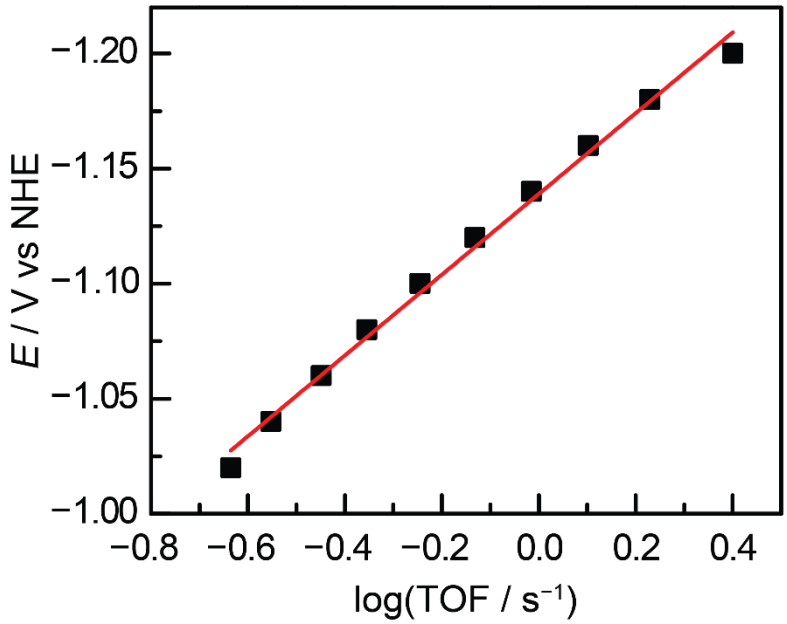

Figure S11. Average of two potentiostatic Tafel data runs for HER collected with GCC-Rh in 0.1 M NaOH electrolyte. The slope of the best fit line is 176 mV dec^{-1}.

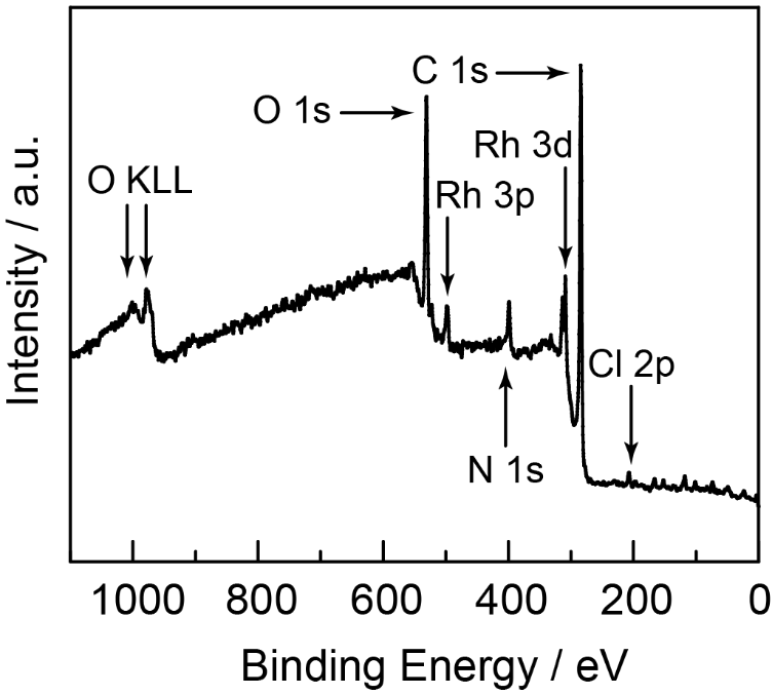

Figure S12. XPS survey spectrum GCC-Rh after polarization at –0.51 V vs NHE for 10 minutes in 0.1 M perchloric acid (pH 1.1).

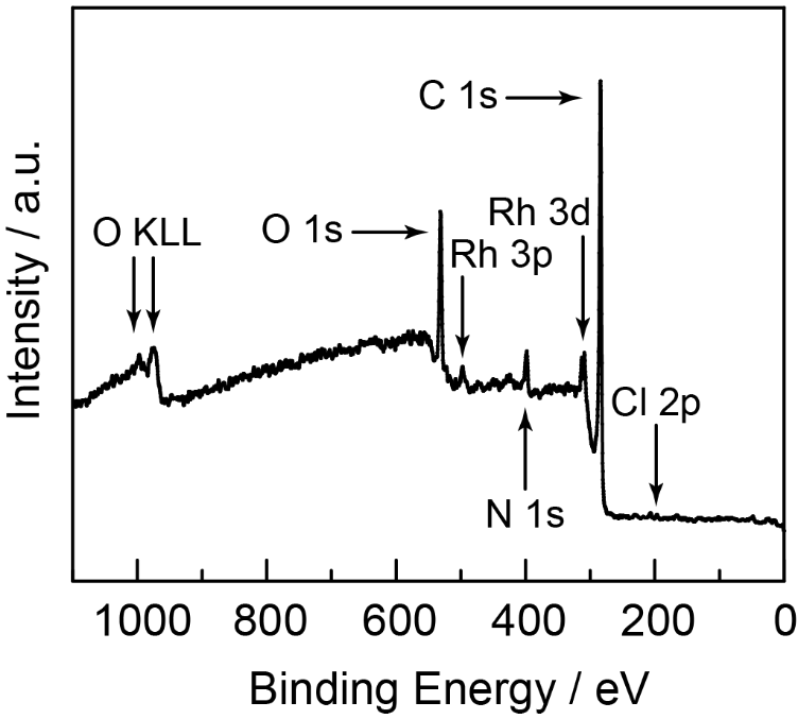

Figure S13. XPS survey spectrum GCC-Rh after polarization at –0.58 V vs NHE for 10 minutes in 0.1 M sodium formate (pH 2.2).

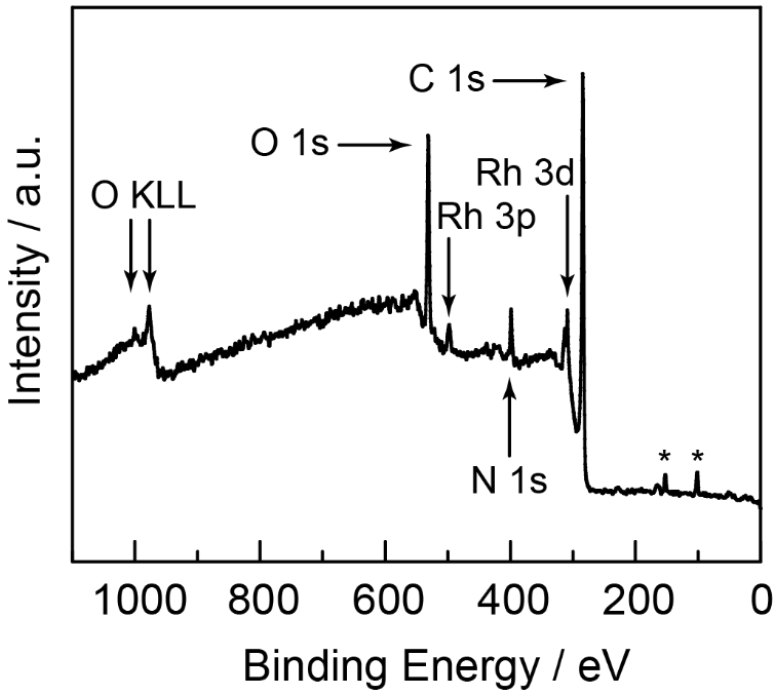

Figure S14. XPS survey spectrum GCC-Rh after polarization at –0.87 V vs NHE for 10 minutes in 0.1 M sodium phosphate (pH 7.1). *indicates adventitious Si impurities.

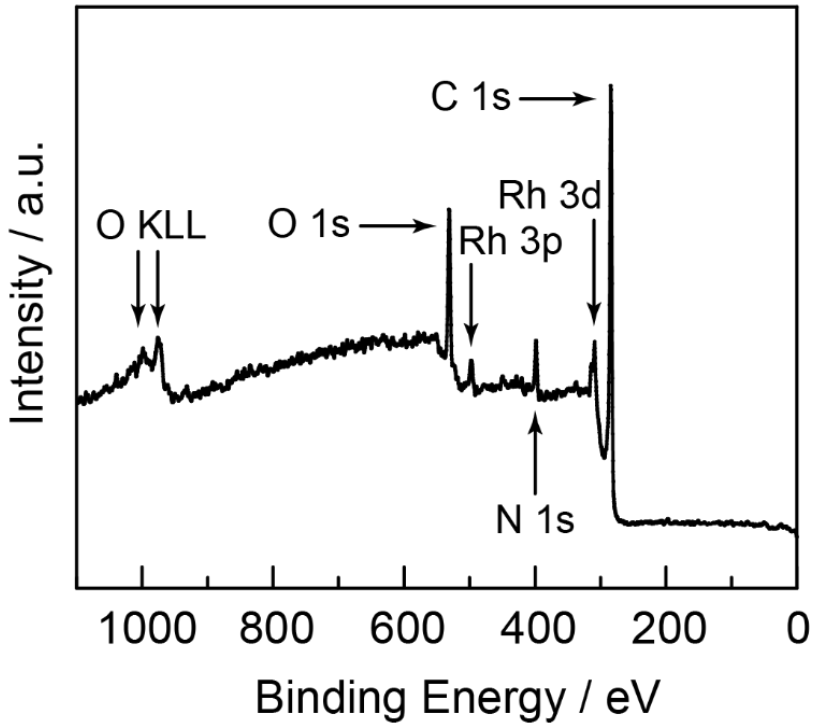

Figure S15. XPS survey spectrum GCC-Rh after polarization at –0.99 V vs NHE for 10 minutes in 0.1 M sodium borate (pH 9.2).

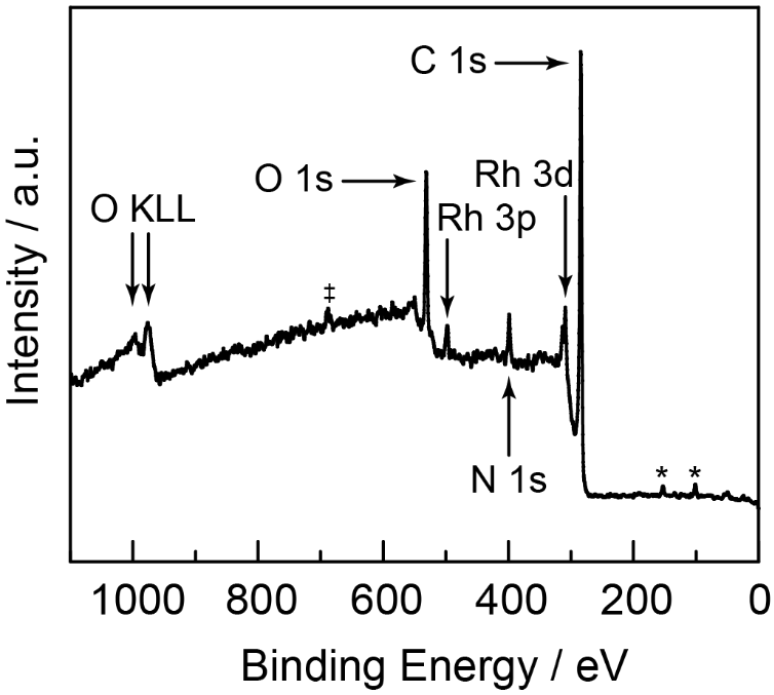

Figure S16. XPS survey spectrum GCC-Rh after polarization at –1.20 V vs NHE for 10 minutes in 0.1 M sodium hydroxide (pH 12.8). ‡indicates adventitious F from Teflon polishing holder and *indicates adventitious Si impurity.

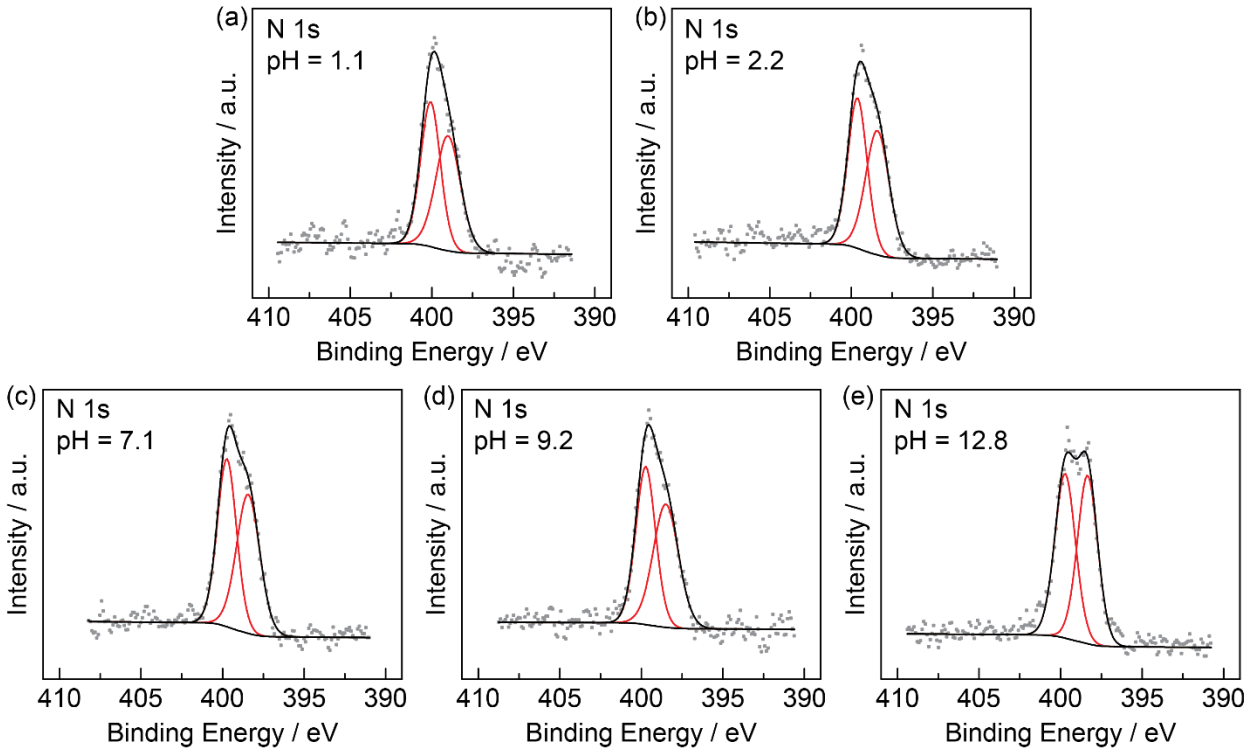

Figure S17. High-resolution N 1s XPS spectrum of GCC-Rh after 10 minutes of polarization in (a) 0.1 M perchloric acid, (b) 0.1 M sodium formate, (c) 0.1 M sodium phosphate, (d) 0.1 M sodium borate, (e) 0.1 M sodium hydroxide. The ratio of pyrazinic to metal-bound pyridinic N species is 1:1. We hypothesize that differences in wave shape are due to interactions between the molecular site on the GCC and different ionic species in different buffers. The measured signal is in gray, the fit background in black, the fit peaks in red, and the overall fit manifold in black.

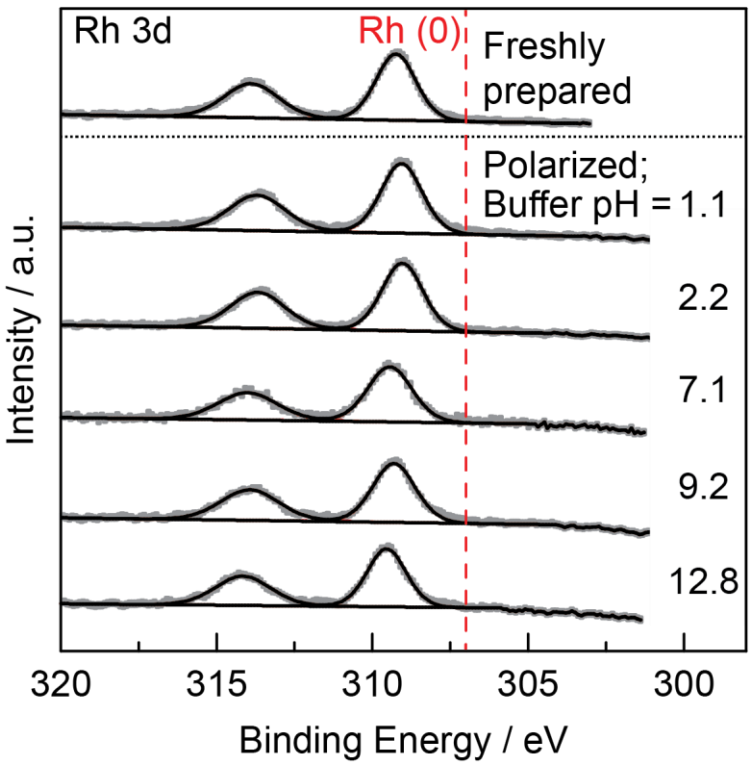

Figure S18. High-resolution XPS spectra of the Rh 3d peak in GCC-Rh freshly prepared (top) and after 10 minutes of polarization at ~0.45 V overpotential in 0.1 M perchloric acid (pH 1.1), 0.1 M sodium formate (pH 2.2), 0.1 M sodium phosphate (pH 7.1), 0.1 M sodium borate (pH 9.2), and 0.1 M sodium hydroxide (pH 12.8). The dotted red line shows the expected binding energy of Rh^0. The measured signal is in gray, and the fit backgrounds and peak manifold are in black.

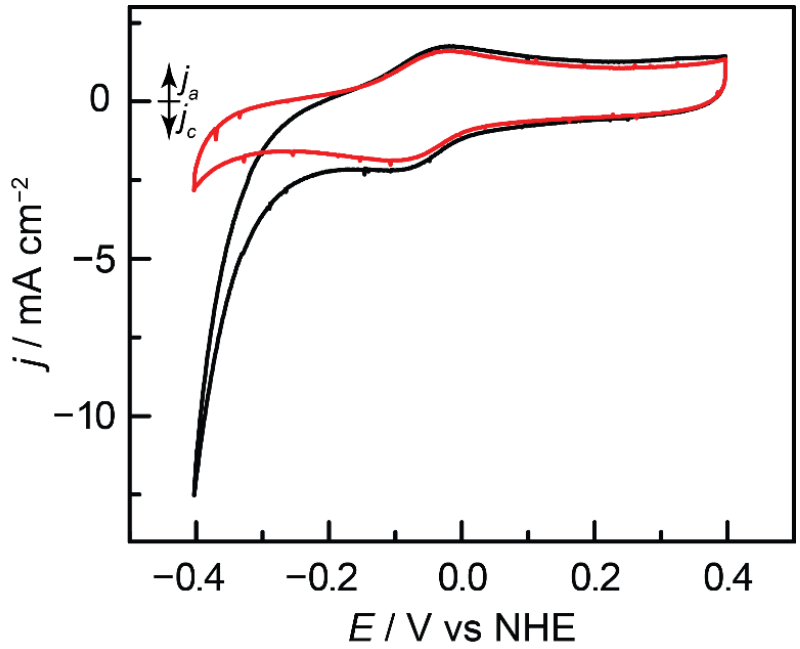

Figure S19. Cyclic voltammograms (10 mV s^{-1}) of GCC-Rh recorded in 0.1 M $HClO_4$ under N_2 (black) and CO (red).

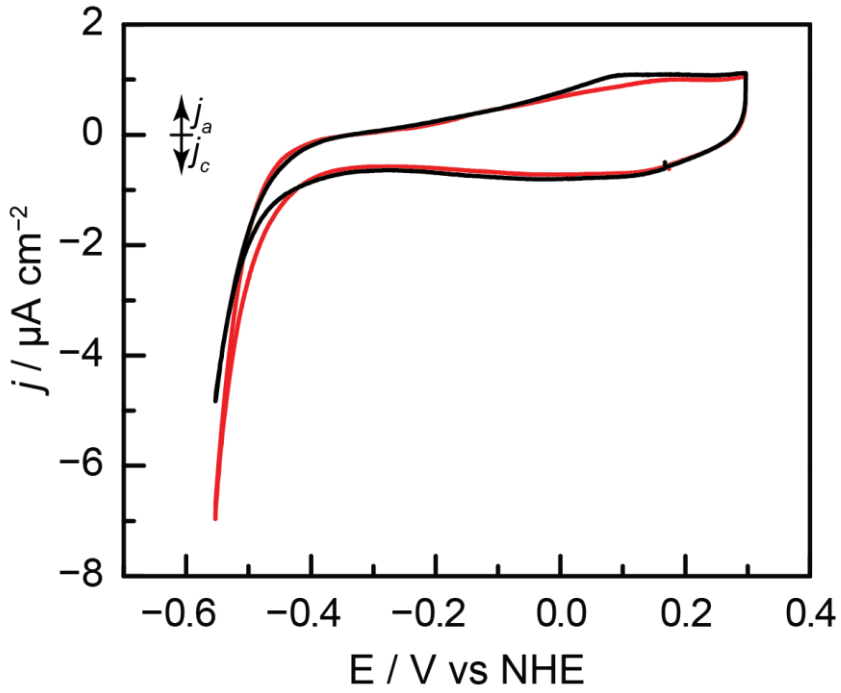

Figure S20. Cyclic voltammograms (10 mV s^{-1}) of GCC-phenazine recorded in 0.1 M $HClO_4$ under N_2 (black) and CO (red).

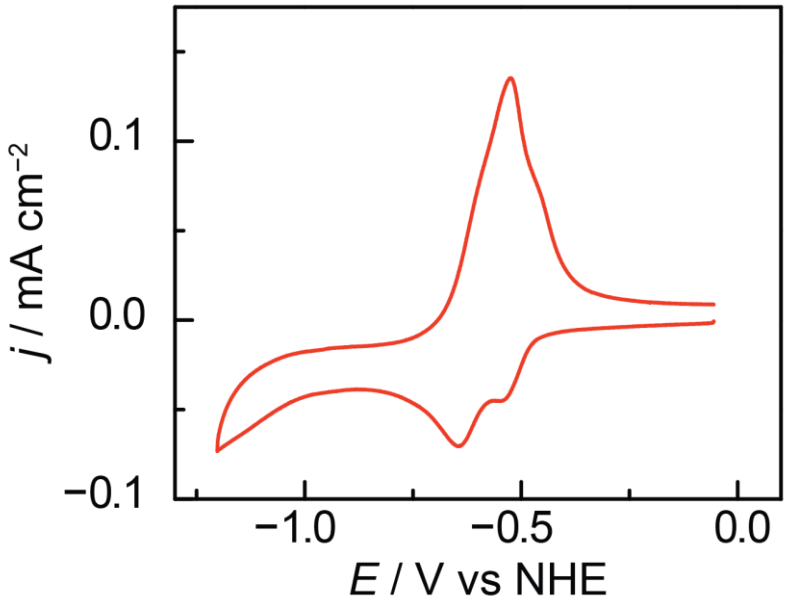

Figure S21. Cyclic voltammogram (100 mV s^{-1}) of 0.3 mM $[RhCp^*(dppz\text{-}SO_3)OH_2]^+$ recorded in 0.1 M sodium hydroxide (pH 13).

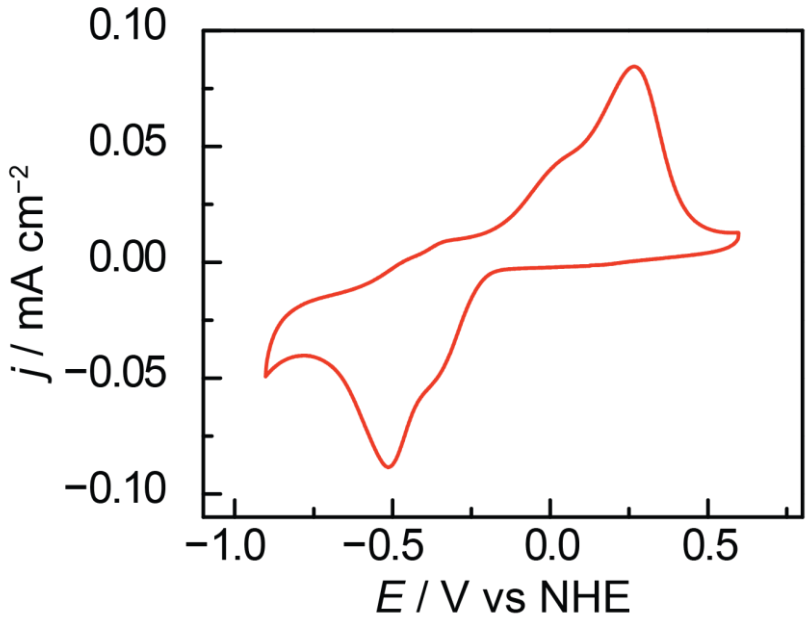

Figure S22. Cyclic voltammogram (100 mV s^{-1}) of 0.3 mM $[RhCp^*(dppz\text{-}SO_3)OH_2]^+$ recorded in 0.1 M sodium phosphate (pH 7).

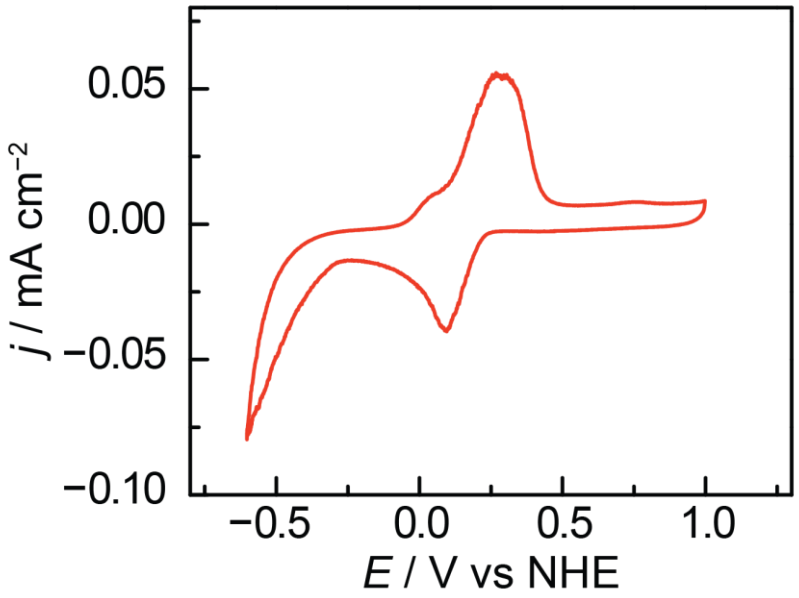

Figure S23. Cyclic voltammogram (100 mV s^{-1}) of 0.3 mM $[RhCp^*(dppz\text{-}SO_3)OH_2]^+$ recorded in 0.1 M perchloric acid (pH 1).

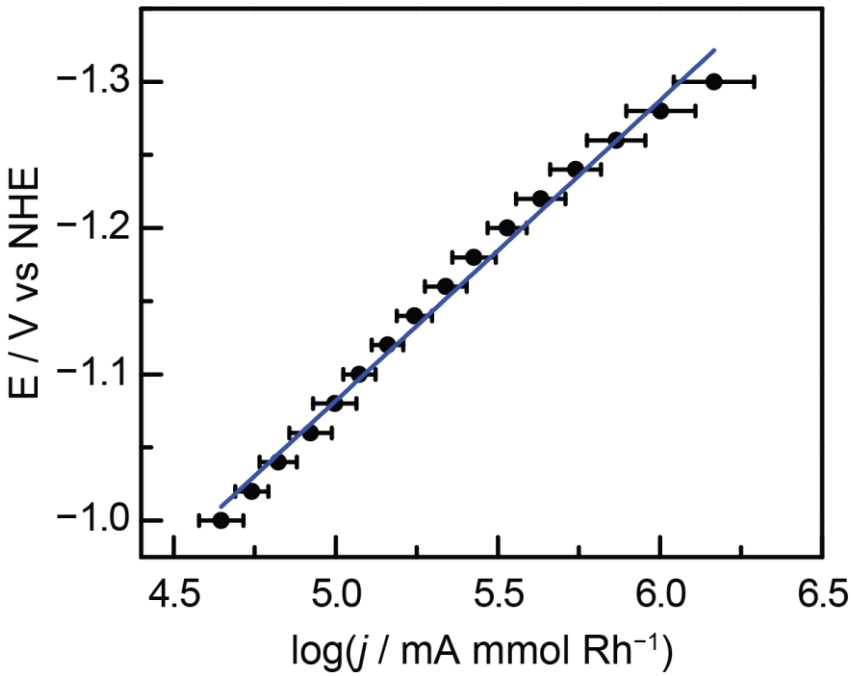

Figure S24. Potentiostatic Tafel data for HER collected with GCC-Rh in 0.1 M NaOH electrolyte. The slope of the best fit line is 200 mV dec^{-1}.

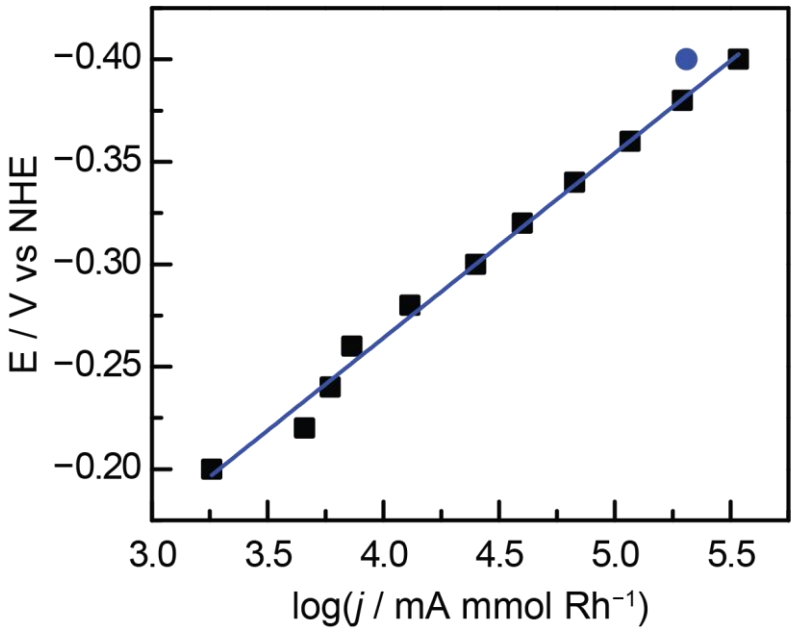

Figure S25. Potentiostatic Tafel data for HER collected with GCC-Rh in 0.1 M $HClO_4$ electrolyte. The black data points were collected in order of increasing potential (decreasing overpotential), and the blue data point was collected at the end of the run. The similarity between the first point collected and the blue point suggest that there is no significant irreversible change in activity over the course of data collection.

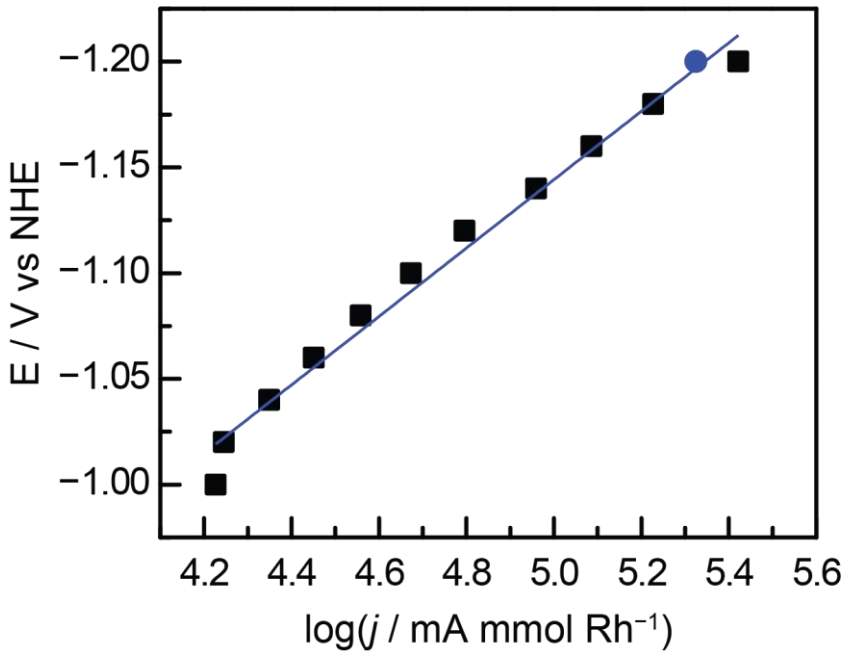

Figure S26. Potentiostatic Tafel data for HER collected with GCC-Rh in 0.1 M NaOH electrolyte. The black data points were collected in order of increasing potential (decreasing overpotential), and the blue data point was collected at the end of the run. The similarity between the first point collected and the blue point suggest that there is no significant irreversible change in activity over the course of data collection.

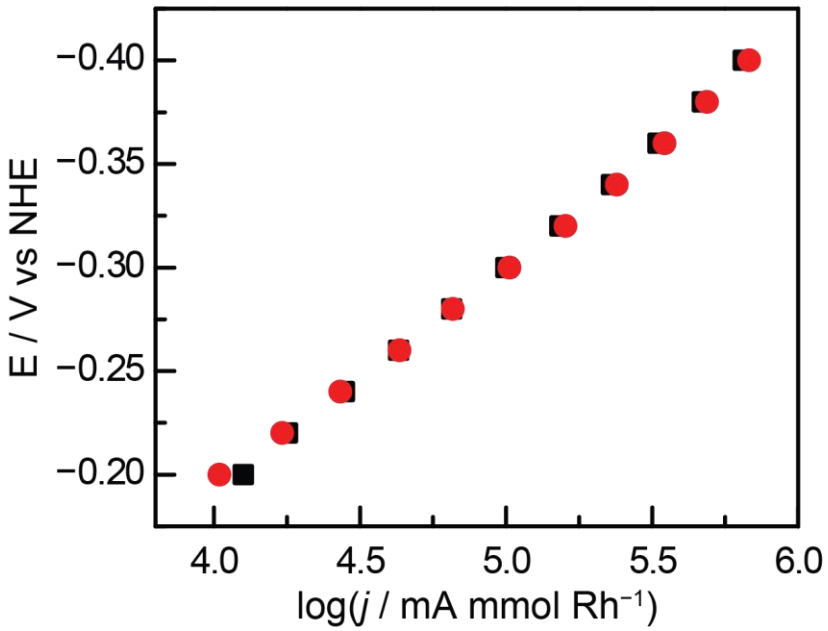

Figure S27. Potentiostatic Tafel data for HER collected with an oxidized GCC-Rh rotating disk electrode in 0.1 M $HClO_4$ electrolyte at 0 rotations per minute (rpm) (black) and 2000 rpm (red). The fact that the red and black data points overlay suggests that the kinetics of hydrogen evolution are not transport limited.

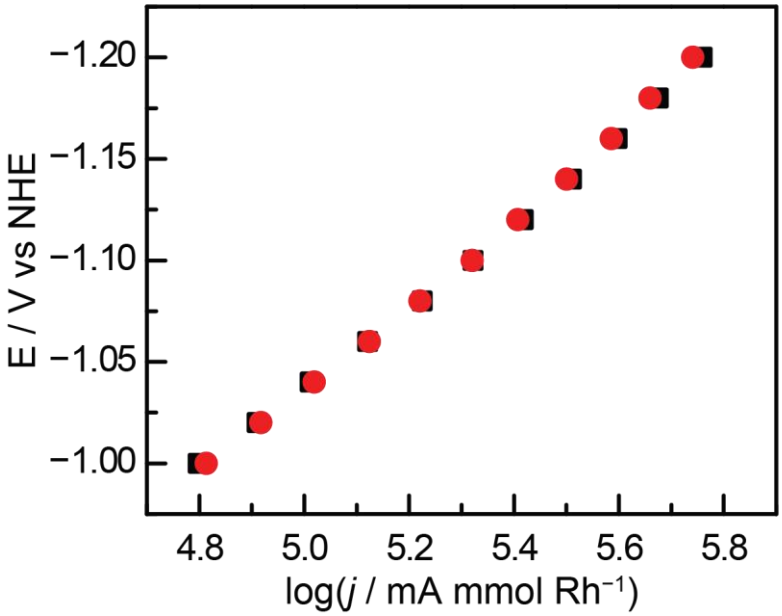

Figure S28. Potentiostatic Tafel data for HER collected with an oxidized GCC-Rh rotating disk electrode in 0.1 M NaOH electrolyte at 0 rotations per minute (rpm) (black) and 2000 rpm (red). The fact that the red and black data points overlay suggests that the kinetics of hydrogen evolution are not transport limited.

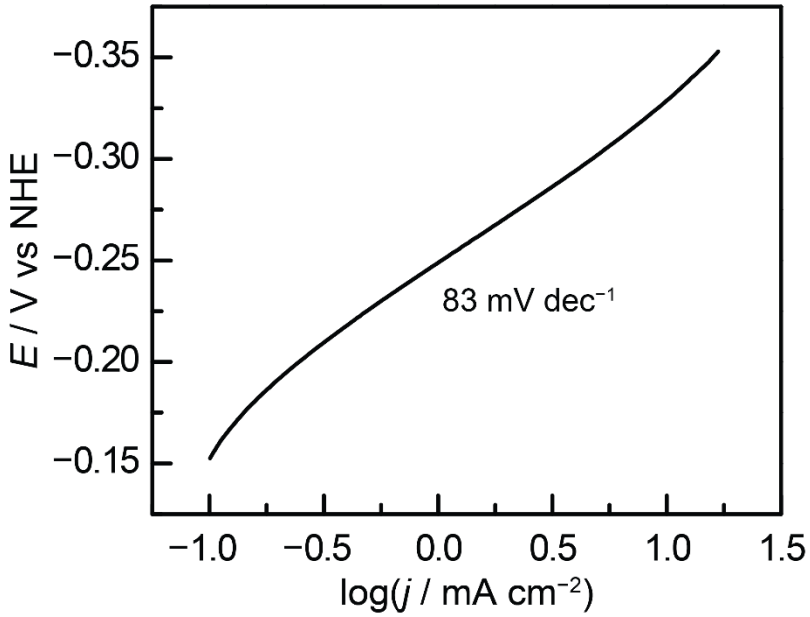

Figure S29. Tafel data for HER replotted from cyclic voltammograms (1 mV s^{-1}) recorded with an oxidized GCC-Rh rotating disk electrode in 1.0 M $HClO_4$ electrolyte. We note that the Tafel slope is the same when the data are recorded at 1 mV s^{-1} and 5 mV s^{-1} (**Figure S32**).

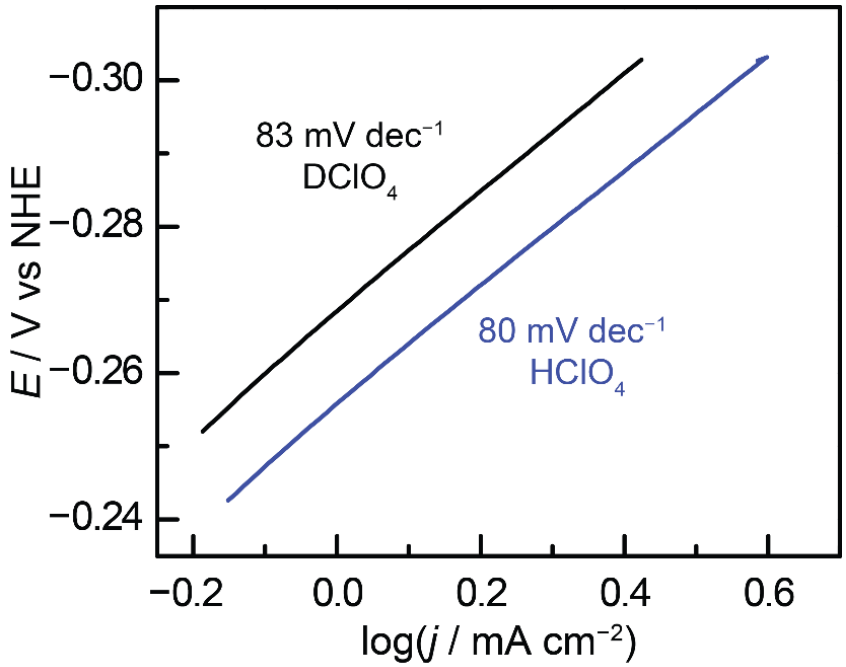

Figure S30. Tafel data for HER replotted from cyclic voltammograms (5 mV s^{-1}) recorded with an oxidized GCC-Rh rotating disk electrode in 1.0 M $HClO_4$ in H_2O (blue) and D_2O (black).

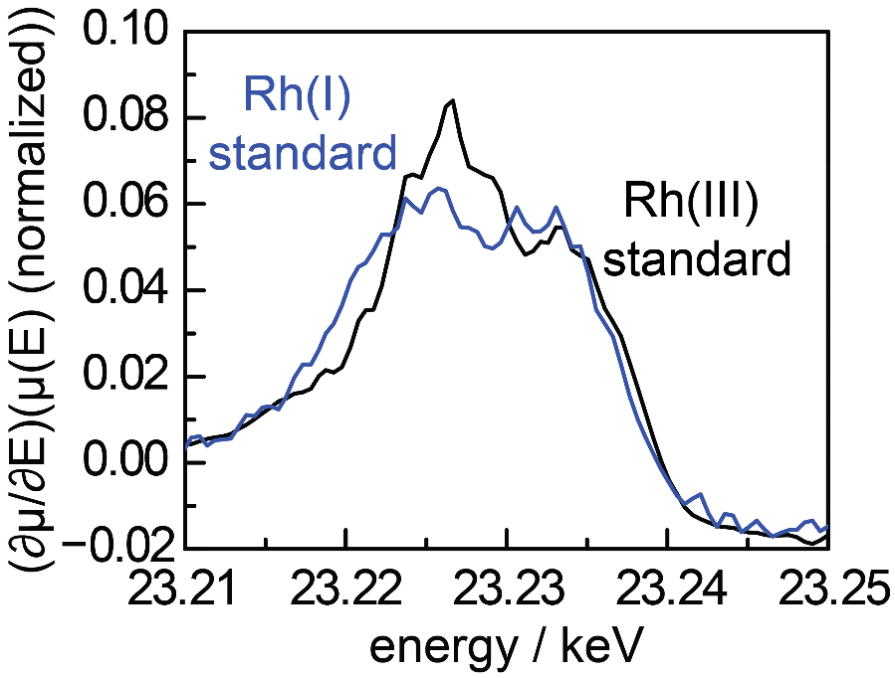

Figure S31. First derivative plot of Rh K-edge X-ray absorption near edge spectra of the Rh(III) standard (black, [RhCp*(phen)Cl]Cl) and the Rh(I) standard (blue, RhCp*(phen)).

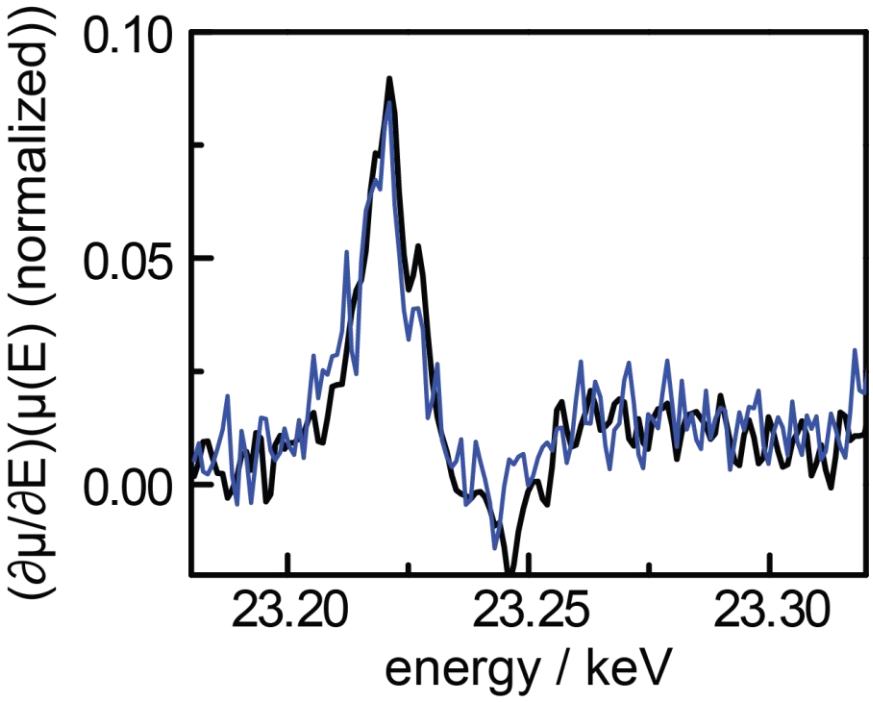

Figure 32. First derivative plot of in situ Rh K-edge X-ray absorption near edge structure spectra of GCC-Rh recorded in 0.1 M NaOH at the open circuit potential (~ 0.15 V vs NHE) (black) and –1.16 V vs NHE (blue).

Table S1: Surface atomic concentrations of GCC-Rh.

GCC-Rh Sample	% N	% Rh	N:Rh ratio
Freshly prepared	7.6 ± 1.70	2.2 ± 0.80	3.5:1
Post-electrolysis pH 1.1	6.32 ± 1.15	1.4 ± 0.34	4.5:1
Post- electrolysis pH 2.2	7.08 ± 1.93	1.58 ± 0.84	4.5:1
Post- electrolysis pH 7.1	6.44 ± 0.27	1.52 ± 0.17	4.2:1
Post- electrolysis pH 9.2	6.11 ± 1.41	1.23 ± 0.33	5.0:1
Post- electrolysis pH 12.8	5.99 ± 0.99	1.11 ± 0.19	5.4:1

Table S2: Rh binding energy in GCC-Rh.

GCC-Rh Sample	Rh binding energy
Freshly prepared	309.4 ± 0.4
Post-electrolysis pH 1.1	309.3 ± 0.4
Post-electrolysis pH 2.2	309.3 ± 0.2
Post-electrolysis pH 7.1	309.3 ± 0.1
Post-electrolysis pH 9.2	309.4 ± 0.1
Post-electrolysis pH 12.8	309.4 ± 0.1
Rh^0 expected binding energy	307.0[2]

References:

(1) Gileadi, E. *Physical Electrochemistry, Fundamentals, Techniques and Applications*; Wiley-VCH: Weinheim, 2011. pp 44−51.

(2) Mouvier, G.; Hoogewys, M.; Leclere, C. X-Ray Photoelectron Spectroscopy and Electron Microscopy of Pt−Rh Gauzes Used for Catalytic Oxidation of Ammonia. *J. Catal.* **1977**, *48*, 217–228.

(3) Pentland, N.; Bockris, J. O.; Sheldon, E. Hydrogen Evolution Reaction on Copper, Gold, Molybdenum, Palladium, Rhodium, and Iron. *J. Electrochem. Soc.* **1957**, *104* (3), 182.

(4) Parsons, R. The Rate of Electrolytic Hydrogen Evolution and the Heat of Adsorption of Hydrogen. *Trans. Faraday Soc.* **1958**, *54*, 1053.

(5) Delahay, P. Double Layer and Electrode Kinetics; Interscience: New York, 1954; pp 260–268.

(6) Costentin, C.; Drouet, S.; Robert, M.; Savéant, J.-M. Turnover Numbers, Turnover Frequencies, and Overpotential in Molecular Catalysis of Electrochemical Reactions. Cyclic Voltammetry and Preparative-Scale Electrolysis. *J. Am. Chem. Soc.* **2012**, *134* (27), 11235–11242.

(7) Bard, A. J.; Faulkner, L. R. *Electrochemical Methods Fundimentals and Applications*, 2nd ed.; John Wiley & Sons, Inc.: New York, NY, 2001, pp. 87−155.

(8) Kleineweischede, A.; Mattay, J. Synthesis of Amino- and Bis(Bromomethyl)-Substitued Bi- and TetradentateN-Heteroaromatic Ligands: Building Blocks for Pyrazino-Functionalized Fullerene Dyads. *European J. Org. Chem.* **2006**, *2006* (4), 947–957.

(9) Bodige, S.; MacDonnell, F. M. Synthesis of Free and Ruthenium Coordinated 5,6-Diamino-1,10-Phenanthroline. *Tetrahedron Lett.* **1997**, *38* (47), 8159–8160.

(10) Kolle, Ulrich; Grutzel, M. Organometallic Rhodium(III) Complexes as Catalysts for the Photoreducton of Protons to Hydrogen on Colloidal TiO_2. *Angew. Chem. Int. Ed. Engl.* **1987**, *26* (6), 567–570.

(11) Aguirre Quintana, L. M.; Johnson, S. I.; Corona, S. L.; Villatoro, W.; Goddard, W. A.; Takase, M. K.; VanderVelde, D. G.; Winkler, J. R.; Gray, H. B.; Blakemore, J. D. Proton – Hydride Tautomerism in Hydrogen Evolution Catalysis. *Proc. Natl. Acad. Sci. U. S. A.* **2016**, *113* (23), 6409–6414.

(12) Blakemore, J. D.; Hernandez, E. S.; Sattler, W.; Hunter, B. M.; Henling, L. M.; Brunschwig, B. S.; Gray, H. B. Pentamethylcyclopentadienyl Rhodium Complexes. *Polyhedron* **2014**, *84*, 14–18.

(13) Pitman, C. L.; Finster, O. N. L.; Miller, A. J. M. Cyclopentadiene-Mediated Hydride

Transfer from Rhodium Complexes. *Chem. Commun.* **2016**, *52*, 9105–9108.
(14) da Silva Miranda, F.; Signori, A. M.; Vicente, J.; de Souza, B.; Priebe, J. P.; Szpoganicz, B.; Gonçalves, N. S.; Neves, A. Synthesis of Substituted Dipyrido[3,2-a:2′,3′-c]Phenazines and a New Heterocyclic Dipyrido[3,2-f:2′,3′-h]Quinoxalino[2,3-b]Quinoxaline. *Tetrahedron* **2008**, *64* (22), 5410–5415.